

1 **The peripheral T cell population is associated with pneumonia severity**
2 **in cynomolgus monkeys experimentally infected with severe acute**
3 **respiratory syndrome coronavirus 2**

4

5 Running title: Pathogenesis of SARS-CoV-2 in a macaque model

6

7 Noriyo Nagata^{1*}, Naoko Iwata-Yoshikawa¹, Kaori Sano¹, Akira Ainai¹, Nozomi Shiwa¹,
8 Masayuki Shirakura², Noriko Kishida², Tomoko Arita², Yasushi Suzuki², Toshihiko Harada³,
9 Yasuhiro Kawai³, Yasushi Ami³, Shun Iida^{1,4}, Harutaka Katano¹, Seiichiro Fujisaki², Tsuyoshi
10 Sekizuka⁵, Hiroyuki Shimizu⁶, Tadaki Suzuki^{1¶}, Hideki Hasegawa^{2¶}

11

12 ¹ Department of Pathology, National Institute of Infectious Diseases, Tokyo, Japan

13 ² Influenza Virus Research Center, National Institute of Infectious Diseases, Tokyo, Japan

14 ³ Management Department of Biosafety and Laboratory Animal, National Institute of Infectious
15 Diseases, Tokyo, Japan

16 ⁴ Division of Infectious Diseases Pathology, Department of Global Infectious Diseases, Tohoku
17 University Graduate School of Medicine, Miyagi, Japan

18 ⁵ Pathogen Genomics Center, National Institute of Infectious Diseases, Tokyo, Japan

19 ⁶ Department of Virology II, National Institute of Infectious Diseases, Tokyo, Japan

20

21 *Corresponding author:

22 E-mail: nnagata@nih.go.jp (NN)

23 ¶These authors contributed equally to this work.

24

25 **Abstract**

26 The coronavirus disease 2019 (COVID-19), caused by severe acute respiratory syndrome
27 coronavirus 2 (SARS-CoV-2), is a global pandemic that began in December 2019.
28 Lymphopenia is a common feature in severe cases of COVID-19; however, the role of T cell
29 responses during infection is unclear. Here, we inoculated six cynomolgus monkeys, divided
30 into two groups according to the CD3+ T cell population in peripheral blood, with two clinical
31 isolates of SARS-CoV-2: one of East Asian lineage and one of European lineage. After initial
32 infection with the isolate of East Asian lineage, all three monkeys in the CD3+ low group
33 showed clinical symptoms, including loss of appetite, lethargy, and transient severe anemia
34 with/without short-term fever, within 14 days post-infection (p.i.). By contrast, all three
35 monkeys in the CD3+ high group showed mild clinical symptoms such as mild fever and loss of
36 appetite within 4 days p.i. and then recovered. After a second inoculation with the isolate of
37 European lineage, three of four animals in both groups showed mild clinical symptoms but
38 recovered quickly. Hematological, immunological, and serological tests suggested that the
39 CD3+ high and low groups mounted different immune responses during the initial and second
40 infection stages. In both groups, anti-viral and innate immune responses were activated during
41 the early phase of infection and re-infection. However, in the CD3+ low group, inflammatory
42 responses, such as increased production of monocytes and neutrophils, were stronger than those
43 in the CD3+ high group, leading to more severe immunopathology and failure to eliminate the
44 virus. Taken together, the data suggest that the peripheral T lymphocyte population is associated
45 with pneumonia severity in cynomolgus monkeys experimentally infected with SARS-CoV-2.

46

47 **Author summary**

48 SARS-CoV-2 infection causes an illness with clinical manifestations that vary from
49 asymptomatic or mild to severe; examples include severe pneumonia and acute respiratory
50 distress syndrome. Lymphopenia, which is common in severe COVID-19 cases, is characterized
51 by markedly reduced numbers of CD4+ T cells, CD8+ T cells, B cells, and natural killer cells.
52 Here, we showed that cynomolgus monkeys selected according to the T cell populations in
53 peripheral blood have different outcomes after experimental infection with SARS-CoV-2. These
54 findings will increase our understanding of disease pathogenesis and may facilitate the
55 development of animal models for vaccine evaluation.

56

57 **Introduction**

58 Coronavirus disease 2019 (COVID-19), caused by a novel human coronavirus called severe
59 acute respiratory syndrome coronavirus 2 (SARS-CoV-2), is a global pandemic that began in
60 December, 2019 after cases of an unknown upper respiratory tract infection were reported in
61 Wuhan, Hubei Province, China [1-3]. The World Health Organization declared a global
62 pandemic on March 11, 2020; since then, the number of confirmed cases and the number of
63 deaths has increased rapidly, reaching over 1 million by the end of September 2020 [4].

64 SARS-CoV-2 causes an illness with clinical manifestations ranging from an
65 asymptomatic or mild infection to a serious illness (i.e., severe pneumonia and acute respiratory
66 distress syndrome) [3, 5, 6]. Pathological studies suggest that SARS-CoV-2 infection of the
67 lower respiratory tract causes disease directly [7, 8]. In addition, high expression of
68 pro-inflammatory cytokines, including IL-6 and IL-1 β , in serum from patients with severe
69 COVID-19 suggest that immunopathological damage caused by an over-exuberant host
70 response might contribute to poor outcomes [3, 9, 10]; this is similar to other coronavirus
71 infections such as SARS and Middle East respiratory syndrome (MERS) [11-15]. Lymphopenia
72 is a common characteristic of severe COVID-19; severe cases show a marked reduction in the
73 numbers of CD4+ T cells, CD8+ T cells, B cells, and natural killer (NK) cells [3, 9, 10].
74 Because T cells may mediate early innate immune responses to virus infection [16],
75 lymphopenia might be associated with severe disease. However, the role of T cell responses
76 during COVID-19 infection is unclear.

77 Several experimental models, including cats, chickens, dogs, ducks, ferrets, mice,
78 hamsters, macaque monkeys, and pigs, have been used to study COVID-19 [17, 18]. Cats,

79 ferrets, human ACE2 transgenic mice, hamsters, and monkeys are all susceptible to
80 SARS-CoV-2 after respiratory inoculation and all exhibit virus excretion from the upper
81 respiratory tract and/or intestine [19-26]. These animals develop acute pulmonary lesions after
82 inoculation with a high dose of virus, but clinical symptoms are mild. As in human cases of
83 SARS, advanced age correlates with adverse outcomes in mice and macaque monkeys [27, 28].
84 However, cynomolgus monkeys do not show age-dependent differences in severity after
85 experimental infection with SARS-CoV-2 [20].

86 Previously, we found that experimental infection of cynomolgus monkeys with
87 human viral pathogens resulted in a few severe cases [29]. Pathophysiological analysis
88 suggested that low populations of lymphocytes were related to the severe clinical symptoms
89 after experimental infection with virus. Thus, we speculated that low T cell populations in
90 peripheral blood might cause poor outcomes after SARS-CoV-2 infection of monkeys. To test
91 this hypothesis, we selected monkeys according to the T cell population in peripheral blood, and
92 infected them with an isolate of SARS-CoV-2 obtained from an individual who returned from
93 Wuhan at the end of January 2020. We then monitored the clinical symptoms, immune
94 responses, and lung pathology. In addition, we examined the effect of a previous infection with
95 SARS-CoV-2 by reinfecing monkeys with a heterologous strain to evaluate whether it
96 enhanced the symptoms of respiratory disease. We did this by re-challenging monkeys with
97 another isolate, a “S-G614 variant strain”, isolated from a returnee from Europe at the end of
98 March 2020. The results suggest that the peripheral T lymphocyte population in peripheral
99 blood is related to severity of pneumonia in cynomolgus monkeys experimentally infected with
100 SARS-CoV-2.

101

102 **Results**

103 **Experimental infection of cynomolgus monkeys with SARS-CoV-2**

104 An overview of the study design is shown in Figure 1A. Twenty-five female monkeys were
105 used. Body weight was measured (S1A Fig) and blood samples obtained for use in a
106 SARS-CoV-2 neutralization assay. All animals except one had undetectable (<1:4) levels of
107 neutralizing antibodies; the exception had a titer of 1:4. The blood samples were also used to
108 investigate the number of lymphocytes and the population of CD3+ cells within the total
109 lymphocyte population (S1B Fig). After assigning animals into "CD3+ high" and "CD3+ low"
110 groups, six cynomolgus monkeys were selected according to body weight (only monkeys
111 weighing 3.5 kg or less were appropriate due to facility restrictions) and CD3+ cell count, and
112 then used in the infection experiments.

113 In this study, we used two isolates of SARS-CoV-2 from Japan: one of East Asian
114 lineage obtained at the end of January 2020, and another of European lineage obtained at end of
115 March 2020 (Table 1).

116

117 **Table 1. Clinical isolates of SARS-CoV-2 used in this study**

Strain	Origin		Accession no.	GISAID	Clade* /	Passage history for the animal experiment in this study		
	Collection date	Specimen				region of exposure	Cell	Propagation
2019-nCoV/Japan /TY	Jan 31, 2020	Throat swab	EPI_ISL_408667	S / East Asia	VeroE6	8 passages**		Negative
/WK-521/2020	Returnee from Wuhan				/TMPRSS2			
hCoV-19/Japan/	29 Mar 2020	Throat swab	EPI_ISL_529135	G / Europe	VeroE6	2 passages		Positive
QH-329-037/2020	Returnee from EU				/TMPRSS2			

118 GISAID, Global Initiative on Sharing All Influenza Data.

119 *GISAID clade referred from "Clade and lineage nomenclature, July 4, 2020"

120 <https://www.gisaid.org/references/statements-clarifications/clade-and-lineage-nomenclature-aids-in-genomic-epidemiology-of-active-hcov-19-viruses/>.

121 **WK-521 was isolated using VeroE6/TMPRSS2 cells unexpectedly contaminated with *Mycoplasma hyorhinis* and *Mycoplasma arginini* (Matsuyama
 122 et al., 2020). Anti-mycoplasma reagents (MC-210, 0.5 µg/mL; Waken, Kyoto, Japan) were used to eradicate mycoplasma contamination from the cells
 123 and virus stock during virus propagation from passages 4 to 6.

124 ***Mycoplasma contamination was detected by PCR (TaKaRa PCR Mycoplasma Detection Set, Takara, Shiga, Japan).

125 The first inoculation with the isolate of East Asian lineage
126 (2019-nCoV/Japan/TY/WK-521/2020, referred to as WK-521) was administered via a
127 combination of the intranasal (0.25 mL, spray into right nostril), conjunctival (0.1 mL, drop on
128 right eye), and intratracheal (1 mL virus solution plus 2 mL saline using a catheter) routes under
129 ketamine-xylazine anesthesia; the monkeys were observed once daily for clinical signs and
130 scored using a clinical scoring system (dietary intake, including pellets and fruits, drinking,
131 attitude in front of regular observers, and stool consistency: the total score was the sum of all
132 five component scores (i.e., 0–5 × 5). (Fig. 1B).

133 All monkeys showed reduced appetite, drank less, and became more lethargic within
134 4–10 days after the initial inoculation. Two animals (#5412 and #5417) from the CD3+ low
135 group showed lower clinical scores than that for the CD3+ high group from 5 to 14 days p.i.
136 Monkey #5412 became lethargic around 10 days after the initial inoculation but ate a piece of
137 fruit every day; therefore, we decided not to euthanize this animal. Indeed, the monkey
138 recovered from severe illness at around 14 days p.i. After the second inoculation with another
139 isolate of European lineage (hCoV-19/Japan/ QH-329-037/2020, referred to as QH-329-037) at
140 35 days after the initial inoculation (referred to as R0d in Fig. 1), all monkeys except #5405
141 showed a reduced clinical score and recovered within 1 week. No obvious body weight loss was
142 observed; indeed, monkey #5405 gained weight (S2A Fig). In all monkeys, body temperature
143 spiked 1 day after the initial inoculation but then returned to normal (the exception was monkey
144 #5405) (S3 Fig). Monkey #5405 continued to have a slightly higher temperature than before the
145 initial inoculation. At 1 day after the second inoculation, two monkeys from the CD3+ high
146 group (#5399 and #5403) showed a spike in body temperature. Biochemical markers (globulin:

147 Glob, albumin: ALB, and glucose) suggested changes in nutritional status after both the initial
148 and second inoculations (S2B Fig).

149 Two monkeys from the CD3+ low group showed low hemoglobin (HGB) levels: one at 7 days
150 (monkey #5417, at the time of planned autopsy) and one at 10 days (monkey #5412) after initial
151 inoculation (Fig. 2A). Red blood cell (RBC) counts and hematocrit levels were also low in these
152 monkeys (S4A Fig).

153

154 **Immune responses in cynomolgus monkeys inoculated with SARS-CoV-2**

155 All monkeys showed transient lymphopenia at 1 day p.i., after which lymphocyte
156 counts increased within the next 7 days (Fig. 2B). After the second inoculation, lymphocyte
157 counts in all monkeys decreased at Day 1 p.i. before recovering again. Mixed-effects models for
158 repeated measures analysis revealed significant differences in the number of lymphocytes
159 between the two groups. By contrast, monocyte counts after the first injection increased before
160 falling again within 7 days p.i. (Fig. 2B). After the second inoculation, monocyte counts did not
161 change significantly. Various changes in the numbers of other leukocytes, including neutrophils,
162 eosinophils, basophils, were seen during infection (S4B Fig).

163 Flow cytometry analysis revealed that changes in the overall lymphocyte count were
164 due to changes in the number of CD3+ T cells (Fig. 2C). In both groups, CD20+ B cell counts
165 dropped at 1 day p.i. and then increased gradually until 28 days p.i., but interestingly, there was
166 a significant difference between CD20+ B cell counts in the CD3+ high and low groups (Fig.
167 2C). After the second inoculation, the number of CD20+ B cells in both groups fell, before
168 increasing again. Three monkeys showed high CD16+ NK cell counts at 4 days after the initial

169 inoculation (Fig. 2C). After the second inoculation, CD16+ NK cells numbers in all monkeys
170 were higher than after the initial inoculation, although numbers remained low in monkey #5412.
171 There was a significant difference in the number of CD3+CD4+ T cells between the two groups
172 (S4C Fig). CD3+ cells, including CD4+ and CD8+ T cell counts, peaked at 7 days after the
173 initial inoculation, but cell numbers increased rapidly after the second inoculation.

174 Levels of IL-6, interleukin 1 receptor antagonist (IL-1ra), monocyte chemotactic
175 protein-1 (MCP-1), IL-15, IL-2, and macrophage inflammatory protein-1 beta (MIP-1 β) in
176 serum peaked at 1 day after the initial inoculation; levels also increased at 1 day after the second
177 inoculation, although the increase was smaller in both groups (Fig. 2D and S5A Fig). Levels of
178 helper T cell (Th cell)-related cytokines, such as IL-12/23 (p40), interferon gamma (IFN- γ),
179 tumor necrosis factor alpha (TNF- α), IL-13, IL-10, and IL-17 increased from Day 10 post-initial
180 inoculation, peaking at Day 14 or 21; expression increased rapidly (within 7 days) after the
181 second inoculation (Fig. 2D and S5B Fig). The kinetics of Th cell-related cytokine responses
182 (except IL-17) were faster in the CD3+ high group than in the CD3+ low group. Dynamic
183 changes in transforming growth factor alpha (TGF- α) and IL-8 levels were also observed in
184 both groups during infection (S5C Fig).

185

186 **Virus shedding by cynomolgus monkeys inoculated with SARS-CoV-2**

187 After the initial inoculation with isolate WK-521, clinical samples (conjunctiva,
188 nasal, throat, and rectal swabs) were collected. Viral RNA was detected by real-time RT-PCR,
189 and infectious virus was detected by culture with TMPRSS2-Vero E6 cells (Fig. 3). The result
190 revealed that two monkeys excreted infectious virus from the upper respiratory tract (nasal and

191 throat swabs from #5404) or intestine (rectal swab from #5412) after the initial inoculation.
192 Real-time RT-PCR confirmed viral replication in the upper respiratory tract and intestine by
193 detecting viral subgenomic mRNAs in swab samples that were positive for viral RNA [30].
194 Actively-infected cells were detected in nasal swabs from two monkeys (#5403 and #5404) and
195 in a rectal swab from one monkey (#5412) (Fig. 3 and S6 Fig). After the second inoculation,
196 none of the monkeys excreted infectious virus, although viral subgenomic mRNA was detected
197 in nasal (#5403) and rectal (#5412) swabs (Fig. 3).

198

199 **Seroconversion after experimental infection with SARS-CoV-2**

200 No monkeys, including #5404 and #5417 euthanized on Day 7 p.i., showed
201 seroconversion within 7 days p.i. Neutralizing antibodies were detected from 10 days (monkey
202 #5399 in the CD3+ high group) or 14 days (the other three monkeys in both groups) after the
203 initial inoculation, peaking at 21 days p.i. in the CD3+ high group and 28 days p.i. in the CD3+
204 low group (Fig. 4A). Within 35 days p.i. (35d/R0d in Fig. 4A), the neutralizing antibody titer in
205 monkeys #5399 and #5403 from the CD3+ high group fell slightly; overall, the antibody titers
206 were higher in the CD3+ low group than in the CD3+ high group. After the second inoculation,
207 neutralizing antibody titers increased rapidly at 4 days (R4d) p.i., peaking at 1:640 at 7 days
208 (R7d) p.i., in all monkeys from both groups. Monkeys #5403 and #5412 were euthanized at R7
209 days p.i. After this time point, the titers in monkeys #5399 and #5405 fell slightly to 1:320 at 14
210 days. Sidak's multiple comparisons test after application of a mixed-effects models for repeated
211 measures analysis revealed a significant difference in neutralizing antibody titers between the
212 two groups. Serum obtained from the monkeys showed cross-reactivity with both strains of

213 virus (S1 Table).

214 We also used in-house IgM, IgA, and IgG enzyme-linked immunosorbent assay (ELISAs) to
215 examine antibody isotypes and their binding to the spike (S), receptor binding domain (RBD),
216 and nucleocapsid (N) proteins (Fig. 4B). At 7 or 10 days p.i., S-, RBD-, and N protein-specific
217 IgM, IgA, and IgG antibody titers increased in both groups. Spearman's correlation analysis
218 revealed that the IgA and IgG responses correlated with the neutralizing antibody response ($R >$
219 0.8). High levels of IgG antibodies specific for the S and RBD proteins were observed in
220 monkey #5412, which showed prolonged excretion of infectious virus from the intestine after
221 the initial inoculation.

222

223 **Transcriptomic analyses of peripheral whole blood from monkeys inoculated with**
224 **SARS-CoV-2**

225 Transcriptomic analyses were conducted using RNA extracted from peripheral whole
226 blood samples collected at different time points: before initial inoculation (Day 0), after initial
227 inoculation (Days 1, 4, and 7), before the second inoculation (R0), and after the second
228 inoculation (R1, R4, and R7). Gene expression was compared between samples collected from
229 animals before (Day 0) and after (Days 1, 4, 7, R0, R1, R4, and R7) virus inoculation to identify
230 differentially expressed genes (S7A Fig). The results revealed that 331 genes were upregulated
231 significantly, while 176 genes were downregulated significantly, after virus infection. Among
232 the 507 differentially expressed genes, 78 were related to the immune response (S7B Fig). Next,
233 we conducted gene set enrichment analyses using samples collected from the CD3+ high and
234 CD3+ low groups after (Days 1, 4, 7, R0, R1, R4, and R7) virus infection (Fig. 5A). Expression

235 of genes encoding neutrophil-, monocyte-, and inflammatory signal-related modules were
236 downregulated to a greater extent in the CD3+ high group than in the CD3+ low group (green
237 dots in Fig. 5A), whereas expression of genes encoding B cell-related modules was upregulated
238 to a greater extent in the CD3+ high group than in the CD3+ low group (gray dots in Fig. 5A).
239 Furthermore, to evaluate differences in transcriptomic profiles over time, we conducted gene set
240 enrichment analyses at baseline (before virus infection, Day 0) and at different time points after
241 virus infection (Days 1, 4, 7, R0, R1, R4, and R7) (Fig. 5B). The results revealed significant
242 upregulation of genes encoding innate anti-viral immune system-related modules (yellow dots
243 in Fig. 5B) on Days 1 and 4 in both the CD3+ high and CD3+ low groups. Of note, upregulation
244 of genes encoding inflammation-related modules (green & red dots in Fig. 5B) and
245 downregulation of genes encoding T cell-related modules (black dots in Fig. 5B) were more
246 prominent in the CD3+ low group than in the CD3+ high group. Upregulation of innate immune
247 response-related genes was observed following re-infection with virus, although no alteration in
248 expression of T cell- and B cell-related genes was observed. Overall, expression of more
249 immune response-related modules was altered significantly in the CD3+ low group compared
250 with the CD3+ high group, suggesting a difference in the magnitude of the immune response
251 between the two groups following virus infection.

252

253 **Distribution of viral RNA in monkey tissues at the experimental end-point**

254 At the experimental end-point, tissue samples were also collected to detect viral
255 RNA, subgenomic mRNA, and infectious virus (Fig. 6 and S6B Fig). Two monkeys (#5404 and
256 #5417) euthanized at 7 days after initial inoculation had viral RNA and/or subgenomic mRNA

257 in the upper and lower lobe of the lungs. At 7 and 14 days after the second inoculation (R7d and
258 R14d), two monkeys (#5412 and #5405) from the CD3+ low group had viral RNA and/or
259 subgenomic mRNA in the lower lobe of the lungs and in the trachea. Monkey #5412 excreted
260 the virus in rectal swabs (Fig. 3) and had detectable viral RNA and/or subgenomic mRNA in the
261 large intestine and mesenteric lymph nodes at 7 days after the second inoculation. High levels of
262 viral RNA were detected in the tonsil and subcarinal lymph nodes of monkeys in both the CD3+
263 high and low groups at various time points. No infectious virus was isolated from tissue samples
264 using TMPRSS2/VeroE6 cells. Because it was difficult to distinguish cytopathic effects (CPE)
265 from cytotoxicity caused by the tissue homogenate, we performed blind passage of
266 TMPRSS2/VeroE6 cells in the presence of culture supernatant from the first inoculation plus
267 10% tissue homogenate; however, there were no distinct CPEs within 5 days p.i., after the
268 second blind passage.

269 As mentioned above, we used a heterologous strain of the virus for the second
270 infection. To identify single nucleotide variations and the major population of virus in monkey
271 tissues, we used the next generation sequencer MiSeq to obtain the entire length of the viral
272 genome. Thirteen RNA samples obtained from tonsil, mesenteric lymph nodes, and lung tissues
273 from infected monkeys were used for analysis; however, four samples did not meet the quality
274 standards. The read number obtained for six samples of tonsil and lung returned only partial
275 viral genome sequences (S2 Table). In the end, only three samples were suitable for genome
276 sequencing; the sequences obtained from these samples were compared with the Wuhan-Hu-1
277 genome sequence (accession no. MN908947.3) as a reference (Table 2). The sequence data
278 have been deposited in the DNA Data Bank of Japan (DDBJ) Sequence Read Archive, under

279 submission ID DRA011219 (BioSample accessions: SAMD00261559 – 00261561). In addition,

280 because the number of reads was sufficient at the D614G position (>200), a genetic population

281 analysis of the D614G variant was performed in six samples (S3 Table).

282

283 **Table 2. SARS-CoV-2 variants in tissue samples from monkeys after experimental infection**

Group	Stain (Accession no.)	Nucleotide position, reference: Wuhan-Hu-1 (accession no. MN908947.3)													
		1648	2662	4185	4456	5497	8782	11942	12334	13548	16596	18755	18804	21886	23403
Region		ORF1a								ORF1b				S	
Nonsynonymous mutation		-	-	G1307A	-	-	-	Q3893*	-	-	-	P1763L	-	-	D614G
1st inoculum	WK-521 (EPI_ISL_408667)	C	T	G	C	C	T	C	A	C	C	C	C	T	A
CD3+ high at 7 dpi	#5404_Tonsil (SAMD00261560)	-	-	-	-	-	-	-	-	-	-	-	-	-	-
CD3+ low at R7 dpi	#5412_Lung (SAMD00261561)	T	-	-	T	T	T	-	del	T	T	T	T	-	-
	#5412_Mesenteric lymph node (SAMD00261559)	100%*			100%	62%	60%		100%	100%	100%	51%	50%		
		-	-	C	-	-	-	T	-	-	-	-	-	C	-
				61%*				55%							100%
2nd inoculum	QH-329-037 (EPI_ISL_529135)	-	C	-	-	-	C	-	-	-	-	-	-	-	G

284 *Percent nucleotide polymorphism; del, deletion.

285

286 The results revealed that the viral genome obtained from the tonsil of monkey #5404
287 after initial inoculation did not harbor any mutations (threshold = 50%). However, the viral
288 genome isolated from the lung of monkey #5412 harbored nine single nucleotide
289 polymorphisms (SNPs), including seven silent point mutations, one deletion resulting in a
290 frameshift mutation in the ORF1ab region, and a nonsynonymous mutation in ORF1b. The most
291 common base change was C > T. In addition, the genome isolated from mesenteric lymph nodes
292 from monkey #5412 harbored three SNPs, including two nonsynonymous mutations in the
293 ORF1a region and a synonymous mutation in the S region. The major sequence in these two
294 isolates was derived from WK-521, suggesting that the original inoculum replicated and resided
295 in the respiratory tract and intestine of monkey #5412, even after the second inoculation with
296 the heterologous strain. The viral genome obtained from the tonsil of monkey #5403 after the
297 second inoculation harbored a D614G mutation in the S region, suggesting the presence of
298 QH-329-037 in the tonsil after the 2nd inoculum (S3 Table). The viral genome also obtained
299 from the tonsil of #5405 after the second inoculation harbored a D614G mutation in the S
300 region, suggesting the presence of QH-329-037 in the tonsil. Interestingly, the genome obtained
301 from the subcarinal lymph node of monkey #5405 did not harbor the D614G mutation,
302 suggesting that the original inoculum was maintained in the accessory lymph node of the lungs.
303 These results suggest that the initially inoculated virus (WK-521) was maintained in the lungs
304 and/or accessory lymph nodes, and that the second inoculated virus (QH-329-037) was
305 eliminated from the lungs of these monkeys soon after the second inoculation.

306

307 **Pathology of SARS-CoV-2 infection in cynomolgus monkeys inoculated with**

308 **SARS-CoV-2**

309 Gross pathology of lungs from monkeys at each end-point is shown in Fig. 7A.

310 Obvious gross lung lesions observed in monkey #5417 at 7 days after the initial inoculation

311 (Fig. 7A, red and white arrows). After the second inoculation, enlargement of the subcarinal

312 lymph nodes was seen in three monkeys, except #5405 (Fig. 7A, yellow arrows).

313 Histopathological analysis revealed varying degrees of alveolar damage in monkeys #5404 and

314 #5417 at 7 days after the initial inoculation (Fig. 7B). Lung tissue from monkey #5404 showed

315 multifocal, slight to mild, interstitial pneumonia, with mononuclear cell aggregates in the

316 alveoli (Fig. 7B, upper row). Monkey #5417 developed more severe interstitial pneumonia, with

317 pulmonary edema comprising degenerated cells and polymorphonuclear leukocytes (Fig. 7B,

318 lower row). Proliferating type II cells overlying the pulmonary walls were observed within the

319 lesions. CD3+ lymphocytes and CD68+ macrophages were present in the alveoli. The lesions in

320 the lungs of monkey #5417 contained predominantly CD68+ macrophages rather than CD3+

321 cells (Fig. 7C).

322 Double immunohistochemistry revealed high expression of ACE2 on the surface of the

323 pulmonary bronchi, but staining was very weak in the alveoli (S8 Fig, upper row); there was no

324 merging of virus antigen (S8 Fig, brown) and ACE2 (S8 Fig, green) signals in either area. In

325 addition, ACE2 was strongly expressed by hyperplastic type II pneumocytes in the pulmonary

326 lesions (S8 Fig, lower row).

327 Monkeys euthanized after the second inoculation had slight focal interstitial

328 inflammation, with macrophages and lymphocytes in the alveoli but no evidence of viral

329 antigens (S9 Fig).

330 Supplementary figure 10 shows representative examples of histopathology of the
331 lungs and extrapulmonary organs. Hemophagocytosis were seen in the alveoli and lymph nodes
332 from monkey #5417, which showed severe anemia at 7 days p.i. (S10A Fig). Diffuse
333 eosinophilic and plasma cell infiltration was seen in the mesenteric lymph nodes, small
334 intestines and large intestine from monkey #5412, which showed prolonged viral excretion after
335 initial infection (S10B Fig). No viral antigens were detected in extrapulmonary tissues.

336

337 **Discussion**

338 In our previous study of the SARS-CoV HKU39849 isolate, we inoculated six
339 cynomolgus monkeys via the intranasal, intragastric, intravenous, or intratracheal routes and
340 found that only intratracheal inoculation with 10^8 TCID₅₀ virus in 5 mL of medium induced
341 acute pneumonia [31]. A low dose (10^3 TCID₅₀ in 3.5 mL) administered intranasally failed to
342 establish an infection, whereas a high dose (10^6 TCID₅₀ in 3.5 mL) succeeded; indeed, infection
343 was detected in nasal and throat swabs within 7 days post-inoculation. In addition, an
344 epidemiological study suggests that COVID-19-associated conjunctivitis is a possible
345 transmission route for SARS-CoV-2 [32]. Therefore, in this study we used a combined
346 inoculation protocol comprising the nasal, intratracheal, and conjunctive routes, and used a high
347 titer of SARS-CoV-2. Shed virus was detected in the upper respiratory and intestinal tracts of
348 infected monkeys, but not consistently (even in nasal and throat swabs); however, one monkey
349 from the CD3+ low group showed prolonged shedding of virus in rectal swabs. Other macaque
350 models infected with clinical isolates of SARS-CoV-2 show similar results [20, 33]. One of
351 these studies showed that viral RNA levels in throat and nasal swabs from young cynomolgus

352 monkeys peaked at Day 1 or 2 post-inoculation; however, they peaked at Day 4 in older
353 monkeys [20]. A few conjunctival swab samples were positive for viral RNA, but not for
354 subgenomic mRNA; in addition, none of the monkeys developed obvious conjunctivitis during
355 the observation period in this study. Taken together, these data suggest that a combination of the
356 intranasal and intratracheal routes (at least) might be appropriate for vaccine studies. In
357 addition, a previous study suggests that the presence of subgenomic mRNA in throat and/or
358 nasopharyngeal swabs should be considered when testing vaccine efficacy [34]. Our own study
359 using young adult cynomolgus monkeys suggests that peripheral T lymphocytes (CD3+) are
360 associated with pneumonia severity. Thus, it is important to consider both the age of the
361 individual and T cell population when selecting animals for vaccine studies [18].

362 Peripheral blood lymphocyte subsets in humans are affected by factors such as
363 gender, age, and ethnicity, and by lifestyle factors such as stress [35]. In this study, we used
364 young healthy monkeys, which showed a wide range of peripheral CD3+ cells. The immune
365 system of non-human primates may also be affected by environmental and physiological
366 conditions [36, 37].

367 According to an epidemiological study of COVID-19, about 10% of the global
368 population may be infected by October 2020; however, most infected people are asymptomatic
369 or mildly symptomatic [38]. That said, some people develop severe pneumonia resulting in
370 respiratory failure, sepsis, and even death (the current fatality rate is 0.15–0.20%). Similar to
371 SARS-CoV and MERS-CoV, older age is a risk factor for severe SARS-CoV-2. Whereas
372 absolute lymphopenia is not specific to COVID-19, low CD3+, CD4+, and CD8+ T cell counts
373 in peripheral blood have been observed in severe cases of COVID-19 [39]. These cases also

374 present with comorbidities such as chronic underlying diseases. Zheng et al. reported that the
375 total CD3+ count is lower in both mild and severe cases of COVID-19 than in healthy controls,
376 but that CD3+, CD8+, and NK cell counts are significantly lower in severe cases [40]. In
377 addition, functional exhaustion (e.g., reduction of CD107a expression and IFN- γ , IL-2, and
378 TNF- α production by CTLs and NK cells) occurred in severe cases.

379 Murine models of SARS-CoV and MERS-CoV infection suggest that failure to
380 induce an early IFN-I response leads to severe pathology and disease [41, 42]. Sera from
381 hospitalized COVID-19 patients show reduced IFN-I and -III levels in response to
382 SARS-CoV-2, but a significant increase in inflammatory chemokines and cytokines [43]. In the
383 current study, transcriptome analysis revealed that innate anti-viral immune responses occurred
384 during the early phase of infection in both the CD3+ high and low groups. In both groups, IRF2,
385 which regulates type I IFN production, was activated during the early phase of infection and
386 upon re-infection. However, in the CD3+ low group, inflammation overwhelmed the T cell
387 response. This is supported by the kinetics of T cell-associated cytokine and chemokine
388 production in monkey sera. Thus, a strong inflammatory response, coupled with a weak/delayed
389 T cell response, was critical for the development of more severe SARS-CoV-2 in the CD3+ low
390 group. By contrast, an early type I IFN-related innate immune response controlled viral
391 replication and dispersion at an early stage in the CD3+ high group.

392 On Days 7–10 after the initial inoculation, two monkeys from the CD3+ low group
393 became lethargic, with decreased hemoglobin levels and RBC counts suggestive of severe
394 anemia. In some cases of COVID-19, low hemoglobin levels indicate anemia [2, 44-46]. The
395 mechanism underlying anemia in COVID-19 patients is unclear; however, virus infection and

396 inflammation impact iron metabolism [47-49]. Levels of serum ferritin, an intracellular protein
397 that maintains iron levels, mirror the degree of inflammation in infectious diseases. In this
398 study, we did not measure ferritin levels in blood from infected monkeys; however, studies
399 show that hospitalized COVID-19 patients have high ferritin levels [2, 46]. The impact of
400 anemia and high ferritin levels on outcome after SARS-CoV-2 infection is unclear [45]. In this
401 study, one of two monkeys (#5417) with anemia that was sacrificed for planned autopsy showed
402 severe acute pneumonia and hemophagocytosis in the cervical lymph nodes. Another (#5412)
403 showed extreme lethargy and anemia on Day 10; however, the monkey ate a piece of apple
404 despite showing loss of appetite. Therefore, we continued to observe this animal until recovery
405 within 14 days p.i., at which point seroconversion occurred. Monkey #5412 showed a low
406 clinical score and excreted infectious virus from intestine for 3 weeks.

407 Pathological evaluation revealed varying degrees of virus infection and host response
408 in the lungs of SARS-CoV-2-infected monkeys at 7 days p.i. Morphologically, SARS-CoV-2
409 replicated in epithelial cells in the pulmonary bronchus and alveoli of monkey #5404, resulting
410 in mild pneumonia. Similar to SARS-CoV infection, expression of ACE2 and SARS-CoV
411 antigen-positive cells did not overlap [50]. In a severe case (monkey #5417), pulmonary edema
412 was observed, suggesting severe damage to pneumocytes. The pathological features were early
413 stage diffuse alveolar damage, with hyaline membranes and a few multinucleated giant cells,
414 similar to human cases of SARS and COVID-19 [7, 9, 11, 51-53]. Activated macrophages
415 rather than lymphocytes were seen in the alveoli of monkey #5417, suggesting that massive
416 inflammatory reactions were induced in the lungs. Lack of an active immune response and
417 epithelial regeneration results in a poor outcome [51]. In this study, we used young monkeys;

418 many regenerated type II cells were seen in the lungs of monkey #5417, and high levels of
419 seroconversion occurred in monkey #5412, even from CD3+ low groups.
420 Most infected people are asymptomatic or show mild symptoms during SARS-CoV-2 infection;
421 thus some researchers wonder whether SARS-CoV-2 infection triggers protective immunity
422 against re-infection [54]. A rhesus macaque model clarified that SARS-CoV-2 infection results
423 in protective immunity against re-infection [55]. The latest study reporting human cases of
424 COVID-19 indicate that the neutralizing antibodies against SARS-CoV-2 last only for a few
425 months [56]. The results of the present study suggest the magnitude of neutralizing antibody
426 titers in infected monkeys is dependent on disease severity, similar to human cases [56]. In
427 addition, these monkeys developed a rapid immune response against a second infection with
428 another challenge strain. NK cell and IL-17 responses, suggesting involvement of Th17 cells,
429 were stronger after the second infection than after the initial infection. Transcriptome analysis
430 revealed that upregulation of innate immune responses, rather than T and B cell responses, in
431 the CD3+ low group contributed to a marked reduction in viral replication and less severe
432 pathology, even after a second infection. Seroconversion in monkeys is common after acute
433 virus infections; indeed, we found virus-specific IgM, IgG, and IgA antibodies in the sera. IgM
434 antibodies appeared together with IgG and, later, IgA; however, titers decreased within 3 weeks
435 after inoculation. This result is similar to that of a human cohort study reporting co-induction of
436 IgM and IgG during SARS-CoV infection [57]. SARS-CoV-2-specific IgG antibodies are
437 predominantly specific for the S-/RBD- and N proteins. IgG levels in symptomatic groups are
438 significantly higher than those in asymptomatic groups during the acute phase [58].
439 Asymptomatic cases also show lower levels of pro- and anti-inflammatory cytokines. Similar to

440 human cases of COVID-19, our monkeys showed different immune responses and even
441 seroconversion. After the second inoculation, all monkeys generated high titers of virus-specific
442 IgA and IgG, suggesting re-infection.

443 In this study, we used two clinical isolates of SARS-CoV-2, one from East Asia and
444 one from Europe. After identification of the first case of COVID-19 in Japan on January 15,
445 2020, an epidemiological study of the SARS-CoV-2 genome revealed that the primary clusters
446 identified in January and February in Japan were related to the Wuhan-Hu-1 isolates from China
447 [59]. Soon after the primary wave from China, we faced a second wave of COVID-19 cases
448 caused by lineages imported by returnees from Europe and North America. Thus, we based the
449 infection experiments in this study on the current situation in Japan. We found that previous
450 infection with a Wuhan-Hu-1-related isolate of SARS-CoV-2 led to a less severe illness upon
451 re-infection with a heterologous strain (an S-G614 variant from Europe).

452 We also determined the mutation patterns in SARS-CoV-2 isolates from the lung of
453 monkey #5412 at 6 weeks after the initial inoculation. The most common base changes were C >
454 T, which were synonymous variants in the ORF1ab region of the monkey isolate. This
455 nucleotide substitution is common in SARS-CoV-2 genomes isolated from humans [60, 61]. C
456 > T transitions are thought to be induced by cytosine deaminases [60].

457 Taken together, the data presented herein suggest that a low CD3+ T cell count in
458 peripheral blood might be an important risk factor for more severe COVID-19. We
459 acknowledge that the study has some limitations; the small number of monkeys (due to ethical
460 reasons) in particular. However, the data suggest that the peripheral T lymphocyte population is
461 associated with severity of pneumonia caused by SARS-CoV-2 infection.

462 **Materials and methods**

463 **Ethical statements**

464 All animal experiments complied with Japanese legislation (Act on Welfare and
465 Management of Animals, 1973, revised in 2012) and guidelines under the jurisdiction of the
466 Ministry of Education, Culture, Sports, Science and Technology, Japan (Fundamental
467 Guidelines for Proper Conduct of Animal Experiment and Related Activities in Academic
468 Research Institutions, 2006). Animal care, housing, feeding, sampling, observation, and
469 environmental enrichment were performed in accordance with these guidelines. Every possible
470 effort was made to minimize suffering. The protocols were approved by the committee of
471 biosafety and animal handling and by the committee of ethical regulation of the National
472 Institute of Infectious Diseases, Japan (authorization nos. 519004-I, -II, and -III for monkey
473 experiments; authorization no. 119176 for rabbit immunizations). Each monkey was housed in a
474 separate cage at the National Institute of Infectious Diseases, Japan, and all received standard
475 primate feed and fresh fruit daily, and had free access to water. Each rabbit was housed in a
476 separate cage at the National Institute of Infectious Diseases, Japan, and all received standard
477 rabbit feed and had free access to water. Animal welfare was observed on a daily basis.
478 Inoculation of monkeys with virus was conducted under ketamine-xylazine anesthesia
479 (intramuscular injection of a mixture of 50 mg/mL ketamine and 20 mg/mL xylazine [2:1; 0.2
480 mL/kg]). Sampling procedures were conducted under anesthesia (10 mg/kg ketamine;
481 intramuscular injection). Monkeys were sacrificed under excess anesthesia with ketamine
482 (intramuscular injection). Rabbits were sacrificed under excess anesthesia with pentobarbital
483 sodium (64.8 mg/kg intravenous injection).

484

485 **Biological safety**

486 All work with SARS-CoV-2 was conducted under biosafety level-3 (BSL-3)
487 conditions in the National Institute of Infectious Diseases, Japan. All experimental animals were
488 handled in a biosafety level 3 animal facility in accordance with the guidelines of this
489 committee (approval no. 19-60, 20-1). Animals were contained in a glovebox system in the
490 ABSL-3 facility during experimental infection. All personnel used respiratory protection when
491 handling infectious samples (respirator type N95). Surface disinfection was performed using
492 80% ethanol, while liquids, solid waste, cages, and animal wastes were steam sterilized in an
493 autoclave.

494

495 **Cells and viruses**

496 VeroE6/TMPRSS2 cells and SARS-CoV-2 human isolates were kindly prepared and
497 provided by Dr. Shutoku Matsuyama and Dr. Makoto Takeda (Department of Virology III,
498 National Institute of Infectious Diseases, Japan) [62]. Cells were cultured in Dulbecco's
499 modified Eagle's medium (DMEM, low glucose (Sigma-Aldrich, St. Louis, MO)) containing
500 5% fetal bovine serum (FBS), 50 IU/mL penicillin G, and 50 µg/mL streptomycin (5DMEM).
501 The virus strains used in this study are shown in Table 1. Stocks of the
502 2019-nCoV/Japan/TY/WK-521/2020 isolate (refer as WK-521) of SARS-CoV-2 (accession no.
503 EPI_ISL_408667) and the hCoV-19/Japan/QH-329-037/2020 isolate (refer as QH-329-037)
504 were propagated eight times or twice, respectively, and titrated on VeroE6/TMPRSS2 cells in
505 DMEM containing 2% FBS (2DMEM).

506 Whole-genome amplification of strain QH-329-037 was carried out using the
507 modified version of ARTIC Network's protocol for SARS-CoV-2 genome sequencing by
508 replacing some of the primers for multiplex PCR [63]. A next generation sequencing (NGS)
509 library was constructed using the QIAseq FX DNA library kit (Qiagen, Hilden, Germany) and
510 sequenced using the NextSeq 500 platform (Illumina, San Diego, CA). NGS reads were mapped
511 to the SARS-CoV-2 Wuhan-Hu-1 reference genome sequence (GenBank accession no.
512 MN908947) using bwa mem [64], followed by trimming the primer region by
513 "trim_primer_parts.py" (https://github.com/ItokawaK/Alt_nCov2019_primers). For
514 determination of the nearly full-length genome sequence, the trimmed reads were assembled
515 using A5-miseq v.20140604 [65]. The full genome sequence of strain QH-329-037 has been
516 deposited in the Global Initiative on Sharing All Influenza Data database (GISAID) under
517 accession ID EPI_ISL_529135.

518 To eradicate mycoplasma contamination, cells and strain WK-521 were treated with
519 an anti-mycoplasma reagent, MC-210 (0.5 µg/mL; Waken, Kyoto, Japan). Mycoplasma
520 contamination was confirmed by PCR using the TaKaRa PCR Mycoplasma Detection Set
521 (Takara, Shiga, Japan).

522

523 **Animal experiments**

524 Twenty-five female adult cynomolgus macaques (*Macaca fascicularis*) imported
525 from China were purchased from Hamri Co., Ltd (Ibaraki, Japan) in 2018 and maintained in the
526 animal facility of the National Institute of Infectious Diseases, Japan. At around 4 weeks before
527 experimental infection, blood samples were collected from all animals under anesthesia with

528 ketamine (intramuscular injection) (Fig. 1A). Sera were used for neutralization assays against
529 SARS-CoV-2. Ethylenediaminetetraacetic acid (EDTA) blood samples were used for
530 hematologic tests and flow cytometry analysis. Six monkeys (young adult females, 5 years old)
531 were selected for experimental infection with SARS-CoV-2. At 14 days before inoculation with
532 the virus, a small implantable thermo logger (DST micro-T: 8.3 × 25.4 mm; Star-oddi,
533 Gardabaer, Iceland) was set intraperitoneally under ketamine anesthesia. The loggers were
534 retrieved at necropsy. Six monkeys were transferred to the animal facility at biosafety level 3
535 and allowed to acclimatize for 1 week. The animals were observed daily for clinical signs
536 (dietary intake, including pellets and fruits, drinking, attitude in front of regular observers, and
537 stool consistency) using a standardized scoring system until the end of the study. Scoring was
538 performed as follows: daily intake of pellets (0–5), fruits including orange and apple (0–5), and
539 drinking water (0–5), attitude in front of regular observers (i.e., standing up, show interest in the
540 outside, getting attention, intimidation, up and down movement: 0–5), stool consistency (color,
541 stiffness, form, volume, frequency: 0–5). The total score was the sum of all five component
542 scores.

543 The six monkeys were anaesthetized by intramuscular injection of a mixture of 50
544 mg/mL ketamine and 20 mg/mL xylazine (2:1; 0.2 mL/kg). After collecting samples, including
545 blood and swabs, monkeys were inoculated with an isolate of SARS-CoV-2 (WK-521) via the
546 intranasal (0.125 mL, sprayed into the right nostril; Keytron, Ichikawa, Japan), conjunctival (0.1
547 mL dropped into the right eye), and intratracheal (1 mL of virus solution plus 2 mL of saline via
548 a catheter; 6Fr; Atom Medical, Tokyo, Japan) routes (all three routes combined). On Days 0, 1,
549 4, 7, 10, 14, 21, 28, and 35 after initial virus inoculation, clinical samples (conjunctiva, nasal,

550 throat, and rectal swabs, and blood samples) were collected after monkeys were weighed under
551 anesthesia. Two animals were euthanized at 7 days post-initial inoculation, and four animals
552 were re-inoculated with another isolate of SARS-CoV-2 (QH-329-037) at 35 days p.i. After
553 re-inoculation, two animals were euthanized at 7 days post-second inoculation (R7 days p.i.),
554 and the remaining two were euthanized at R14 days p.i. Clinical samples were collected at R1,
555 R4, R7, R10, and R14 days p.i.

556

557 **Virus titration**

558 Tissue samples in Lysing Matrix tubes containing beads (Lysing Matrix A; MP
559 Biomedicals, Irvine, CA) were homogenized using a mini Bead-Beater (Biospec Products,
560 Bartlesville, OK) at 100 rpm for 30 sec (twice), and then diluted in 2×DMEM to yield 10%
561 homogenates. After centrifugation at 10,000 \times g for 1 min at 4°C, the supernatants were used for
562 titration on VeroE6/TMPRSS2 cells. Swab samples were also used for titration. Inoculated cells
563 were assessed for CPE at 5 days p.i. The detection limit was $10^{1.5}$ TCID₅₀/mL 10% tissue
564 homogenate or swab sample.

565

566 **Real-time RT-PCR of SARS-CoV genome and detection of viral sequence**

567 Total RNA was extracted from 100 μ L swab samples, tissue homogenates, or blood
568 samples using a TRIzol™ Plus RNA Purification Kit (Thermo Fisher Scientific, Waltham, MA)
569 and used to quantify the SARS-CoV-2 genome. On-column PureLink DNase (Thermo Fisher
570 Scientific) treatment was performed during RNA purification, and RNA samples were dissolved
571 in 30 μ L RNase-free water. The viral RNA copy number in samples from monkeys was

572 estimated by real-time RT-PCR [66]. Subgenomic viral RNA transcripts were also detected in N
573 gene transcripts. The primer and probe sets are shown in S4 Table. Real-time RT-PCR was
574 performed using the QuantiTect Probe RT-PCR Kit (QuantiTect, Qiagen, Venlo, Netherlands)
575 and a LightCycler 480 (Roche, Basal, Switzerland) or Mx3005P (Stratagene, La Jolla, CA)
576 apparatus. The thermal cycling conditions were as follows: 50°C for 30 min, 95°C for 15 min,
577 and 45 cycles at 95°C for 15 s and 60°C for 1 min (N2 primer and probe set); or 50°C for 30
578 min, 95°C for 15 min, and 40 cycles of 94°C for 15 s and 60°C for 1 min (N1 set and the
579 sgRNA transcript primer and probe sets).

580 Some samples containing high viral RNA copy numbers were sent for viral sequence
581 analysis by gene analysis services (Takara Bio, Shiga, Japan). The next generation sequencing
582 (NGS) library was prepared using the SuperScript IV First-Strand Synthesis System (Thermo
583 Fisher Scientific), Q5 Hot Start DNA Polymerase (New England Biolabs, Ipswich, MA), and
584 the QIAseq FX DNA Library Kit (Qiagen). The viral genome region was amplified specifically
585 by multiplex PCR [63], and the entire sequence of the viral genome was obtained using the next
586 generation sequencer MiSeq (Illumina, San Diego, CA) with a read length of 250 nt. FASTQ
587 data were imported into the CLC Genomics Workbench (version 11, Qiagen), and the sequence
588 reads were aligned to the reference sequence Wuhan-Hu-1 (accession no. MN908947.3). The
589 threshold variant frequency was 50%. The amino acid substitutions were analyzed on
590 NextClade (<https://clades.nextstrain.org/>). Genome sequences were deposited in the DNA Data
591 Bank of Japan (DDBJ) (<https://www.ddbj.nig.ac.jp/index.html>).

592

593 **Hematological analysis**

594 Complete blood cell counts, hematocrit, and hemoglobin levels in peripheral blood
595 collected in EDTA tubes were measured by an autoanalyzer (VetScan HM2; ABAXIS, Union
596 City, CA). Neutrophil, lymphocyte, monocyte, eosinophil, and basophil counts were measured
597 by microscopic analysis. Blood biochemistry (Glob, ALB, glucose, alkaline phosphatase (ALP),
598 and blood urea nitrogen (BUN)) of lithium-heparin treated whole blood samples was analyzed
599 using the VetScan VS2 (ABAXIS).

600

601 **Flow cytometric analyses**

602 Flow cytometry analysis was conducted to determine the number of T, B, NK,
603 CD4+, and CD8+ cells in peripheral blood samples from monkeys. Cell staining was performed
604 using the NHP T/B/NK Cell Cocktail (Becton Dickinson (BD) Company, Franklin Lakes, NJ)
605 and the NHP T Lymphocyte Cocktail (BD), according to the manufacturer's instructions. After
606 treatment with BD FACS lysing solution (BD), samples were analyzed by flow cytometry using
607 a BD FACSCanto II analyzer (BD). Flow cytometry data were analyzed using FlowJo software
608 (v10.7.1, FlowJo LLC, Ashland, OR).

609

610 **Histopathology and immunohistochemistry**

611 Animals were euthanized by exsanguination under excess ketamine anesthesia and
612 then necropsied. Tissue samples were immersed in 10% phosphate-buffered formalin,
613 embedded in paraffin, sectioned, and stained with hematoxylin and eosin.
614 Immunohistochemical analysis was performed using a polymer-based detection system
615 (Nichirei-Histofine Simple Stain Human MAX PO®; Nichirei Biosciences, Inc., Tokyo, Japan).

616 Antigen retrieval from formalin-fixed monkey tissue sections was performed by autoclaving in
617 retrieval solution (pH 6.0; Nichirei Biosciences) at 121°C for 10 min. Hyper-immune rabbit
618 serum raised against the GST-tagged N protein of SARS-CoV-2 (produced in-house) was used
619 as the primary antibody to detect viral antigens. Peroxidase activity was detected with
620 3,3'-diaminobenzidine (Sigma-Aldrich, St. Louis, MO). Hematoxylin was used for
621 counterstaining. The polyclonal antibody against GST-tagged N protein of SARS-CoV-2 was
622 prepared as follows: first, the recombinant N protein was constructed by inserting the N gene of
623 SARS-CoV-2 into the pGEX-6P vector (GenScript Japan, Tokyo, Japan). Next, the amino acid
624 sequence was optimized to the bacterial codon. The vector was then used to transform
625 *Escherichia coli* strain BL21 (Takara Bio, Shiga, Japan). Expression of the GST-N protein of
626 SARS-CoV-2 was induced by isopropyl-D-1-thiogalactopyranoside (0.3 mM IPTG, Takara
627 Bio). The cell pellets were sonicated, and the inclusion bodies containing the fusion protein
628 were collected. The fusion proteins were extracted from SDS-PAGE gels after reverse staining
629 (AE-1310 EzStain Reverse, Atto, Tokyo, Japan), concentrated using a spin column (Pall
630 centrifugal device 0.2 µm, Pall Corporation, Port Washington, NY), and diluted in PBS using
631 Amicon Ultra-0.5mL Centrifugal Filters (Ultracel-50k). Two New Zealand White rabbits (1.5
632 kg < body weight; female; SLC, Shizuoka, Japan) were immunized (four times at 2-week
633 intervals) with the purified protein conjugated to TiterMax Gold (Sigma-Aldrich). Rabbits were
634 sacrificed under excess anesthesia with pentobarbital sodium (64.8 mg/kg), and whole blood
635 was collected by cardiac puncture using an 18 G needle. After separating sera by centrifugation,
636 IgG was purified from the rabbit serum using a Melon Gel IgG Spin Purification Kit (Thermo
637 Fisher Scientific) and then used for immunohistochemistry.

638

639 **Neutralization assay**

640 During the observation period, blood was obtained under anesthesia with ketamine.

641 Serum samples were collected by centrifugation and inactivated by heating to 56°C for 30 min.

642 Serum samples were titrated (in duplicate) from 1:10 to 1:1280 in 96-well plates and reacted

643 with 100 TCID₅₀ of SARS-CoV-2 (WK-521 or QH-329-037) at 37°C for 1 h before addition of

644 VeroE6/TMPRSS2 cells. Cells were incubated at 37°C for 5 days and examined twice for

645 evidence of viral CPEs. The neutralizing antibody titer was determined as the reciprocal of the

646 highest dilution at which no CPE was observed.

647

648 **ELISAs**

649 To assess the specificity of the IgM, IgA, and IgG antibodies produced by the

650 infected monkeys, recombinant SARS-CoV-2 trimeric spike, RBD, or nucleocapsid protein

651 were used as antigens in ELISAs. Briefly, 96-well assay plates (Corning Inc., Corning, NY)

652 were coated overnight at 4°C with 50 ng recombinant protein in coating buffer (pH 9.6). The

653 serum samples were serially diluted (4-fold from 1:400 to 1:409600) in 5% skim milk in PBS

654 (pH 7.2) containing 0.05% Tween 20 (Sigma-Aldrich) (PBS-T). The well contents were

655 discarded and diluted serum samples were added to the plate. After incubation for 1 h at 37°C,

656 the plate was washed three times with PBS-T. The wells were then incubated with an

657 HRP-conjugated goat anti-monkey IgM antibody (KPL #5220-0334, SeraCare Life Sciences,

658 Inc. Milford, MA, 1/5000, 50 µL/well), an HRP-conjugated goat anti-monkey IgA antibody

659 ((KPL #5220-0332, SeraCare Life Sciences, 1/5000, 50 µL/well), or an HRP-conjugated goat

660 anti-monkey IgG heavy and light chain antibody (A140-102P, 1/10000, 50 µL/well, Thermo
661 Fisher Scientific) in 5% skim milk in PBS-T for 1 h at 37°C. After three washes with PBS-T, an
662 ABTS substrate (Roche, Basel, Switzerland) was added to the wells, and the plates were
663 incubated for 30 min at room temperature. The optical density (OD) of each well was measured
664 at 405 nm using a microplate reader (Model 680, Bio-Rad). The mean OD value plus three
665 standard deviations ($2 \times \text{mean} + 3 \times \text{SD}$) was calculated using serum samples from pre-infected
666 monkeys and was used as the cut-off for the Ig ELISAs.

667

668 **Detection of inflammatory cytokines and chemokines**

669 All serum samples tested in the BSL2 laboratory (all of which were confirmed
670 negative for viral RNA by RT-PCR) were irradiated for 1 min with UV-C light. Cytokine and
671 chemokine levels in monkey sera were measured using a MILLIPLEX MAP Non-Human
672 Primate Cytokine Magnetic Bead Panel - Premixed 23 Plex - Immunology (Milliplex MAP kit,
673 Merck Millipore, Burlington, MA), which includes the following 23 cytokines and chemokines:
674 G-CSF, granulocyte macrophage colony-stimulating factor (GM-CSF), interferon gamma
675 (IFN- γ), IL-1ra, IL-1 β , IL-2, IL-4, IL-5, IL-6, IL-8, IL-10, IL-12/23 (p40), IL-13, IL-15, IL-17,
676 IL-18, monocyte chemotactic protein-1 (MCP-1), macrophage inflammatory protein 1 alpha
677 (MIP-1 α), MIP-1 β , sCD40L, transforming growth factor alpha (TGF- α), tumor necrosis factor
678 alpha (TNF- α), and vascular endothelial growth factor. The assay samples were read on a
679 Luminex 200TM instrument with xPONENT software (Merck Millipore), as described by the
680 manufacturer.

681

682 **RNA sequencing and data analyses**

683 Whole blood was collected from animals at multiple time points using PAXgene
684 Blood RNA Tubes (PreAnalytiX, Hombrechtikon, Switzerland). Tubes were frozen at -80°C
685 until RNA extraction. RNA was extracted using PAXgene Blood RNA Kits (PreAnalytiX) and
686 shipped to Macrogen Corp. Japan (Kyoto, Japan) for NGS sequencing. Next, cDNA libraries
687 were prepared using a TruSeq Stranded Total RNA LT Sample Prep Kit (Illumina) in
688 accordance with the TruSeq Stranded Total RNA Sample Prep Guide (Part #15031048 Rev. E
689 protocol). Next, the cDNA libraries were paired-end sequenced (read length = 101 bp) on a
690 NovaSeq6000 sequencer (Illumina). Raw FASTQ files were quality checked using fastqc
691 v0.11.8 [67], and low-quality bases from paired reads were trimmed using Trimmomatic v0.39
692 [68]. Paired reads were aligned to the *Macaca fascicularis* genome (version 5.0, Ensembl release
693 101) using the STAR aligner v2.7.3a [69] and default settings. Read fragments (paired reads
694 only) were quantified per gene per sample using featureCounts v1.6.0 [70]. All raw RNA seq
695 fastq files were uploaded to the DDBJ Sequence Read Archive (DRA accession number:
696 DRA010881). All functional analyses of transcriptomic data were performed in the R statistical
697 environment (v3.6.2). Significantly differentially expressed genes between samples collected
698 before and after virus infection were identified using DESeq2 v1.26.0 [71] with default settings,
699 and a minimum adjusted *P*-value significance threshold of 0.05. Volcano plots were created
700 from shrunken log2-fold change values for each gene, calculated by DESeq2 (shrinkage type:
701 normal). For the heatmaps, DESeq2-normalized counts per gene were plotted using the heatmap
702 package [72]. Gene set enrichment analyses (GSEA) were conducted using tmod v0.44 [73],
703 with count data normalized with the voom function within the limma package v3.42.2 [74].

704 GSEA (with default settings and a minimum *P*-value significance threshold of 0.01) was
705 conducted between samples collected from animals in the CD3+ high and low groups after virus
706 infection, and samples collected before and at multiple time points after virus infection.

707

708 **Statistical analysis**

709 Data are expressed as the mean and standard error of the mean. Statistical analyses
710 were performed using Graph Pad Prism 8 software (GraphPad Software Inc., La Jolla, CA).
711 Intergroup comparisons (i.e., changes in clinical scores, blood analysis results, and cytokine
712 levels) were performed using Sidak's multiple comparisons test after application of
713 mixed-effects models for repeated measures analysis. The correlation coefficient was evaluated
714 by Spearman's correlation analysis of the neutralization and ELISA test results. A *P*-value of
715 <0.05 was considered statistically significant.

716

717 **Acknowledgements**

718 We thank Dr Shutoku Matsuyama and Dr Makoto Takeda (National Institute of
719 Infectious Disease) for providing VeroE6-TMPRSS2 cells and SARS-CoV-2 isolates. We also
720 thank Dr Masayuki Shimojima, Dr. Hideki Asanuma, Dr Makoto Kuroda, Dr Takushi Nomura,
721 Dr Hiroyuki Yamamoto, Dr Tetsuro Matano, Dr Shinji Watanabe (National Institute of
722 Infectious Diseases), Dr Shintaro Shichinohe, and Dr Kensuke Nakajima (Nagasaki University,
723 Nagasaki, Japan) for helpful discussion. We also thank our colleagues at the Institute, especially
724 Ms Midori Ozaki, Ms Takiko Yoshida, Dr Michiyo Kataoka, Dr. Dai Izawa, and Ms Yuriko
725 Suzuki, for technical assistance.

726

727 **References**

- 728 1. Zhu N, Zhang D, Wang W, Li X, Yang B, Song J, et al. A Novel Coronavirus from Patients with Pneumonia in China, 2019. *N Engl J Med.* 2020;382(8):727-33. Epub 2020/01/25. doi: 10.1056/NEJMoa2001017. PubMed PMID: 31978945; PubMed Central PMCID: PMCPMC7092803.
- 732 2. Chen N, Zhou M, Dong X, Qu J, Gong F, Han Y, et al. Epidemiological and clinical characteristics of 99 cases of 2019 novel coronavirus pneumonia in Wuhan, China: a descriptive study. *Lancet.* 2020;395(10223):507-13. Epub 2020/02/03. doi: 10.1016/S0140-6736(20)30211-7. PubMed PMID: 32007143.
- 736 3. Huang C, Wang Y, Li X, Ren L, Zhao J, Hu Y, et al. Clinical features of patients infected with 2019 novel coronavirus in Wuhan, China. *Lancet.* 2020;395(10223):497-506. Epub 2020/01/28. doi: 10.1016/S0140-6736(20)30183-5. PubMed PMID: 31986264.
- 740 4. JHU. COVID-19 Dashboard by the Center for Systems Science and Engineering (CSSE) at Johns Hopkins University (JHU) 2020.
- 742 5. Chan JF, Yuan S, Kok KH, To KK, Chu H, Yang J, et al. A familial cluster of pneumonia associated with the 2019 novel coronavirus indicating person-to-person transmission: a study of a family cluster. *Lancet.* 2020;395(10223):514-23. Epub 2020/01/28. doi: 10.1016/S0140-6736(20)30154-9. PubMed PMID: 31986261.
- 746 6. Mizumoto K, Kagaya K, Zarebski A, Chowell G. Estimating the asymptomatic proportion of coronavirus disease 2019 (COVID-19) cases on board the Diamond Princess cruise ship, Yokohama, Japan, 2020. *Euro Surveill.* 2020;25(10). Epub 2020/03/19. doi: 10.2807/1560-7917.ES.2020.25.10.2000180. PubMed PMID: 32183930; PubMed Central PMCID: PMCPMC7078829.
- 751 7. Adachi T, Chong JM, Nakajima N, Sano M, Yamazaki J, Miyamoto I, et al. Clinicopathologic and Immunohistochemical Findings from Autopsy of Patient with COVID-19, Japan. *Emerg Infect Dis.* 2020;26(9). Epub 2020/05/16. doi: 10.3201/eid2609.201353. PubMed PMID: 32412897.
- 755 8. Martines RB, Ritter JM, Matkovic E, Gary J, Bollweg BC, Bullock H, et al. Pathology and Pathogenesis of SARS-CoV-2 Associated with Fatal Coronavirus Disease, United States. *Emerg Infect Dis.* 2020;26(9). Epub 2020/05/22. doi:

758 10.3201/eid2609.202095. PubMed PMID: 32437316.

759 9. Xu Z, Shi L, Wang Y, Zhang J, Huang L, Zhang C, et al. Pathological
760 findings of COVID-19 associated with acute respiratory distress syndrome. Lancet
761 Respir Med. 2020;8(4):420-2. Epub 2020/02/23. doi: 10.1016/S2213-2600(20)30076-X.
762 PubMed PMID: 32085846; PubMed Central PMCID: PMCPMC7164771.

763 10. Qin C, Zhou L, Hu Z, Zhang S, Yang S, Tao Y, et al. Dysregulation of
764 Immune Response in Patients With Coronavirus 2019 (COVID-19) in Wuhan, China.
765 Clin Infect Dis. 2020;71(15):762-8. Epub 2020/03/13. doi: 10.1093/cid/ciaa248.
766 PubMed PMID: 32161940; PubMed Central PMCID: PMCPMC7108125.

767 11. Nicholls JM, Poon LL, Lee KC, Ng WF, Lai ST, Leung CY, et al. Lung
768 pathology of fatal severe acute respiratory syndrome. Lancet. 2003;361(9371):1773-8.
769 Epub 2003/06/05. doi: 10.1016/s0140-6736(03)13413-7. PubMed PMID: 12781536;
770 PubMed Central PMCID: PMCPMC7112492.

771 12. Peiris JS, Chu CM, Cheng VC, Chan KS, Hung IF, Poon LL, et al. Clinical
772 progression and viral load in a community outbreak of coronavirus-associated SARS
773 pneumonia: a prospective study. Lancet. 2003;361(9371):1767-72. Epub 2003/06/05.
774 doi: 10.1016/s0140-6736(03)13412-5. PubMed PMID: 12781535; PubMed Central
775 PMCID: PMCPMC7112410.

776 13. Wong CK, Lam CW, Wu AK, Ip WK, Lee NL, Chan IH, et al. Plasma
777 inflammatory cytokines and chemokines in severe acute respiratory syndrome. Clin Exp
778 Immunol. 2004;136(1):95-103. Epub 2004/03/20. doi:
779 10.1111/j.1365-2249.2004.02415.x. PubMed PMID: 15030519; PubMed Central
780 PMCID: PMCPMC1808997.

781 14. Zhang Y, Li J, Zhan Y, Wu L, Yu X, Zhang W, et al. Analysis of serum
782 cytokines in patients with severe acute respiratory syndrome. Infect Immun.
783 2004;72(8):4410-5. Epub 2004/07/24. doi: 10.1128/IAI.72.8.4410-4415.2004. PubMed
784 PMID: 15271897; PubMed Central PMCID: PMCPMC470699.

785 15. Channappanavar R, Perlman S. Pathogenic human coronavirus infections:
786 causes and consequences of cytokine storm and immunopathology. Semin
787 Immunopathol. 2017;39(5):529-39. Epub 2017/05/04. doi: 10.1007/s00281-017-0629-x.
788 PubMed PMID: 28466096; PubMed Central PMCID: PMCPMC7079893.

789 16. Kim KD, Zhao J, Auh S, Yang X, Du P, Tang H, et al. Adaptive immune cells
790 temper initial innate responses. Nat Med. 2007;13(10):1248-52. Epub 2007/09/25. doi:

791 10.1038/nm1633. PubMed PMID: 17891146; PubMed Central PMCID:
792 PMCPMC2435248.

793 17. Lakdawala SS, Menachery VD. The search for a COVID-19 animal model.
794 Science. 2020;368(6494):942-3. Epub 2020/05/30. doi: 10.1126/science.abc6141.
795 PubMed PMID: 32467379.

796 18. Muñoz-Fontela C, Dowling WE, Funnell SGP, Gsell PS, Balta XR, Albrecht
797 RA, et al. Animal models for COVID-19. Nature. 2020. Epub 2020/09/24. doi:
798 10.1038/s41586-020-2787-6. PubMed PMID: 32967005.

799 19. Shi J, Wen Z, Zhong G, Yang H, Wang C, Huang B, et al. Susceptibility of
800 ferrets, cats, dogs, and other domesticated animals to SARS-coronavirus 2. Science.
801 2020;368(6494):1016-20. Epub 2020/04/10. doi: 10.1126/science.abb7015. PubMed
802 PMID: 32269068; PubMed Central PMCID: PMCPMC7164390.

803 20. Rockx B, Kuiken T, Herfst S, Bestebroer T, Lamers MM, Oude Munnink BB,
804 et al. Comparative pathogenesis of COVID-19, MERS, and SARS in a nonhuman
805 primate model. Science. 2020;368(6494):1012-5. Epub 2020/04/19. doi:
806 10.1126/science.abb7314. PubMed PMID: 32303590; PubMed Central PMCID:
807 PMCPMC7164679.

808 21. Jiang RD, Liu MQ, Chen Y, Shan C, Zhou YW, Shen XR, et al. Pathogenesis
809 of SARS-CoV-2 in Transgenic Mice Expressing Human Angiotensin-Converting
810 Enzyme 2. Cell. 2020;182(1):50-8 e8. Epub 2020/06/10. doi:
811 10.1016/j.cell.2020.05.027. PubMed PMID: 32516571; PubMed Central PMCID:
812 PMCPMC7241398.

813 22. Gao Q, Bao L, Mao H, Wang L, Xu K, Yang M, et al. Development of an
814 inactivated vaccine candidate for SARS-CoV-2. Science. 2020;369(6499):77-81. Epub
815 2020/05/08. doi: 10.1126/science.abc1932. PubMed PMID: 32376603; PubMed Central
816 PMCID: PMCPMC7202686.

817 23. Chan JF, Zhang AJ, Yuan S, Poon VK, Chan CC, Lee AC, et al. Simulation
818 of the clinical and pathological manifestations of Coronavirus Disease 2019
819 (COVID-19) in golden Syrian hamster model: implications for disease pathogenesis and
820 transmissibility. Clin Infect Dis. 2020. Epub 2020/03/28. doi: 10.1093/cid/ciaa325.
821 PubMed PMID: 32215622; PubMed Central PMCID: PMCPMC7184405.

822 24. Kim YI, Kim SG, Kim SM, Kim EH, Park SJ, Yu KM, et al. Infection and
823 Rapid Transmission of SARS-CoV-2 in Ferrets. Cell Host Microbe. 2020;27(5):704-9

824 e2. Epub 2020/04/08. doi: 10.1016/j.chom.2020.03.023. PubMed PMID: 32259477;
825 PubMed Central PMCID: PMCPMC7144857.

826 25. Imai M, Iwatsuki-Horimoto K, Hatta M, Loeber S, Halfmann PJ, Nakajima N,
827 et al. Syrian hamsters as a small animal model for SARS-CoV-2 infection and
828 countermeasure development. Proc Natl Acad Sci U S A. 2020;117(28):16587-95. Epub
829 2020/06/24. doi: 10.1073/pnas.2009799117. PubMed PMID: 32571934; PubMed
830 Central PMCID: PMCPMC7368255.

831 26. Hartman AL, Nambulli S, McMillen CM, White AG, Tilston-Lunel NL, Albe
832 JR, et al. SARS-CoV-2 infection of African green monkeys results in mild respiratory
833 disease discernible by PET/CT imaging and shedding of infectious virus from both
834 respiratory and gastrointestinal tracts. PLOS Pathogens. 2020;16(9):e1008903. doi:
835 10.1371/journal.ppat.1008903.

836 27. Roberts A, Paddock C, Vogel L, Butler E, Zaki S, Subbarao K. Aged BALB/c
837 mice as a model for increased severity of severe acute respiratory syndrome in elderly
838 humans. J Virol. 2005;79(9):5833-8. Epub 2005/04/14. doi:
839 10.1128/JVI.79.9.5833-5838.2005. PubMed PMID: 15827197; PubMed Central
840 PMCID: PMCPMC1082763.

841 28. Smits SL, de Lang A, van den Brand JM, Leijten LM, van IWF, Eijkemans
842 MJ, et al. Exacerbated innate host response to SARS-CoV in aged non-human primates.
843 PLoS Pathog. 2010;6(2):e1000756. Epub 2010/02/09. doi:
844 10.1371/journal.ppat.1000756. PubMed PMID: 20140198; PubMed Central PMCID:
845 PMCPMC2816697.

846 29. Nagata N, Saijo M, Kataoka M, Ami Y, Suzuki Y, Sato Y, et al. Pathogenesis
847 of fulminant monkeypox with bacterial sepsis after experimental infection with West
848 African monkeypox virus in a cynomolgus monkey. Int J Clin Exp Pathol.
849 2014;7(7):4359-70. Epub 2014/08/15. PubMed PMID: 25120821; PubMed Central
850 PMCID: PMCPMC4129056.

851 30. Wolfel R, Corman VM, Guggemos W, Seilmaier M, Zange S, Muller MA, et
852 al. Virological assessment of hospitalized patients with COVID-2019. Nature.
853 2020;581(7809):465-9. Epub 2020/04/03. doi: 10.1038/s41586-020-2196-x. PubMed
854 PMID: 32235945.

855 31. Nagata N, Iwata N, Hasegawa H, Sato Y, Morikawa S, Saijo M, et al.
856 Pathology and virus dispersion in cynomolgus monkeys experimentally infected with

857 severe acute respiratory syndrome coronavirus via different inoculation routes. *Int J Exp*
858 *Pathol.* 2007;88(6):403-14. Epub 2007/11/28. doi: 10.1111/j.1365-2613.2007.00567.x.
859 PubMed PMID: 18039277; PubMed Central PMCID: PMCPMC2517337.

860 32. Xia J, Tong J, Liu M, Shen Y, Guo D. Evaluation of coronavirus in tears and
861 conjunctival secretions of patients with SARS-CoV-2 infection. *Journal of Medical*
862 *Virology.* 2020;92(6):589-94. doi: 10.1002/jmv.25725.

863 33. Munster VJ, Feldmann F, Williamson BN, van Doremale N, Perez-Perez L,
864 Schulz J, et al. Respiratory disease in rhesus macaques inoculated with SARS-CoV-2.
865 *Nature.* 2020. Epub 2020/05/13. doi: 10.1038/s41586-020-2324-7. PubMed PMID:
866 32396922.

867 34. Yu J, Tostanoski LH, Peter L, Mercado NB, McMahan K, Mahrokhan SH, et
868 al. DNA vaccine protection against SARS-CoV-2 in rhesus macaques. *Science.*
869 2020;369(6505):806-11. Epub 2020/05/22. doi: 10.1126/science.abc6284. PubMed
870 PMID: 32434945; PubMed Central PMCID: PMCPMC7243363.

871 35. Choi J, Lee SJ, Lee YA, Maeng HG, Lee JK, Kang YW. Reference values for
872 peripheral blood lymphocyte subsets in a healthy korean population. *Immune Netw.*
873 2014;14(6):289-95. Epub 2014/12/22. doi: 10.4110/in.2014.14.6.289. PubMed PMID:
874 25550695.

875 36. Nehete PN, Shelton KA, Nehete BP, Chitta S, Williams LE, Schapiro SJ, et
876 al. Effects of transportation, relocation, and acclimation on phenotypes and functional
877 characteristics of peripheral blood lymphocytes in rhesus monkeys (*Macaca mulatta*).
878 *PLOS ONE.* 2017;12(12):e0188694. doi: 10.1371/journal.pone.0188694.

879 37. Rosso MC, Badino P, Ferrero G, Costa R, Cordero F, Steidler S. Biologic
880 Data of Cynomolgus Monkeys Maintained under Laboratory Conditions. *PloS one.*
881 2016;11(6):e0157003-e. doi: 10.1371/journal.pone.0157003. PubMed PMID:
882 27280447.

883 38. Ioannidis JPA. Global perspective of COVID-19 epidemiology for a
884 full-cycle pandemic. *Eur J Clin Invest.* 2020:e13421. Epub 2020/10/08. doi:
885 10.1111/eci.13423. PubMed PMID: 33026101.

886 39. Nazarullah A, Liang C, Villarreal A, Higgins RA, Mais DD. Peripheral Blood
887 Examination Findings in SARS-CoV-2 Infection. *Am J Clin Pathol.*
888 2020;154(3):319-29. Epub 2020/08/07. doi: 10.1093/ajcp/aqaa108. PubMed PMID:
889 32756872; PubMed Central PMCID: PMCPMC7454310.

890 40. Zheng M, Gao Y, Wang G, Song G, Liu S, Sun D, et al. Functional
891 exhaustion of antiviral lymphocytes in COVID-19 patients. *Cellular & Molecular*
892 *Immunology*. 2020;17(5):533-5. doi: 10.1038/s41423-020-0402-2.

893 41. Channappanavar R, Fehr Anthony R, Vijay R, Mack M, Zhao J, Meyerholz
894 David K, et al. Dysregulated Type I Interferon and Inflammatory
895 Monocyte-Macrophage Responses Cause Lethal Pneumonia in SARS-CoV-Infected
896 Mice. *Cell Host & Microbe*. 2016;19(2):181-93. doi:
897 <https://doi.org/10.1016/j.chom.2016.01.007>.

898 42. Channappanavar R, Fehr AR, Zheng J, Wohlford-Lenane C, Abrahante JE,
899 Mack M, et al. IFN-I response timing relative to virus replication determines MERS
900 coronavirus infection outcomes. *The Journal of Clinical Investigation*.
901 2019;129(9):3625-39. doi: 10.1172/JCI126363.

902 43. Blanco-Melo D, Nilsson-Payant BE, Liu W-C, Uhl S, Hoagland D, Møller R,
903 et al. Imbalanced Host Response to SARS-CoV-2 Drives Development of COVID-19.
904 *Cell*. 2020;181(5):1036-45.e9. doi: 10.1016/j.cell.2020.04.026.

905 44. Fan BE, Chong VCL, Chan SSW, Lim GH, Lim KGE, Tan GB, et al.
906 Hematologic parameters in patients with COVID-19 infection. *American Journal of*
907 *Hematology*. 2020;95(6):E131-E4. doi: 10.1002/ajh.25774.

908 45. Taneri PE, Gómez-Ochoa SA, Llanaj E, Raguindin PF, Rojas LZ, Roa-Díaz
909 ZM, et al. Anemia and iron metabolism in COVID-19: a systematic review and
910 meta-analysis. *European Journal of Epidemiology*. 2020;35(8):763-73. doi:
911 10.1007/s10654-020-00678-5.

912 46. Richardson S, Hirsch JS, Narasimhan M, Crawford JM, McGinn T, Davidson
913 KW, et al. Presenting Characteristics, Comorbidities, and Outcomes Among 5700
914 Patients Hospitalized With COVID-19 in the New York City Area. *JAMA*.
915 2020;323(20):2052-9. doi: 10.1001/jama.2020.6775.

916 47. Kernan KF, Carcillo JA. Hyperferritinemia and inflammation. *Int Immunol*.
917 2017;29(9):401-9. Epub 2017/05/26. doi: 10.1093/intimm/dxx031. PubMed PMID:
918 28541437; PubMed Central PMCID: PMCPMC5890889.

919 48. Wessling-Resnick M. Crossing the Iron Gate: Why and How Transferrin
920 Receptors Mediate Viral Entry. *Annu Rev Nutr*. 2018;38:431-58. Epub 2018/06/01. doi:
921 10.1146/annurev-nutr-082117-051749. PubMed PMID: 29852086; PubMed Central
922 PMCID: PMCPMC6743070.

923 49. Cassat James E, Skaar Eric P. Iron in Infection and Immunity. *Cell Host &*
924 *Microbe.* 2013;13(5):509-19. doi: 10.1016/j.chom.2013.04.010.

925 50. Matsuyama S, Nagata N, Shirato K, Kawase M, Takeda M, Taguchi F. Efficient activation of the severe acute respiratory syndrome coronavirus spike protein
926 by the transmembrane protease TMPRSS2. *J Virol.* 2010;84(24):12658-64. Epub
927 2010/10/12. doi: 10.1128/JVI.01542-10. PubMed PMID: 20926566; PubMed Central
928 PMCID: PMCPMC3004351.

930 51. Mason RJ. Pathogenesis of COVID-19 from a cell biology perspective. *European Respiratory Journal.* 2020;55(4):2000607. doi:
931 10.1183/13993003.00607-2020.

933 52. Nakajima N, Asahi-Ozaki Y, Nagata N, Sato Y, Dizon F, Paladin FJ, et al. SARS coronavirus-infected cells in lung detected by new in situ hybridization
934 technique. *Jpn J Infect Dis.* 2003;56(3):139-41. Epub 2003/08/29. PubMed PMID:
935 12944688.

937 53. Martines R, Ritter J, Matkovic E, Gary J, Bollweg B, Bullock H, et al. Pathology and Pathogenesis of SARS-CoV-2 Associated with Fatal Coronavirus
938 Disease, United States. *Emerging Infectious Disease journal.* 2020;26(9). doi:
939 10.3201/eid2609.202095.

941 54. Ledford H. Coronavirus reinfections: three questions scientists are asking. *Nature.* 2020;585(7824):168-9. Epub 2020/09/06. doi: 10.1038/d41586-020-02506-y.
942 PubMed PMID: 32887957.

944 55. Chandrashekhar A, Liu J, Martinot AJ, McMahan K, Mercado NB, Peter L, et al. SARS-CoV-2 infection protects against rechallenge in rhesus macaques. *Science.*
945 2020. Epub 2020/05/22. doi: 10.1126/science.abc4776. PubMed PMID: 32434946;
946 PubMed Central PMCID: PMCPMC7243369.

948 56. Seow J, Graham C, Merrick B, Acors S, Pickering S, Steel KJA, et al. Longitudinal observation and decline of neutralizing antibody responses in the three
949 months following SARS-CoV-2 infection in humans. *Nature Microbiology.* 2020. doi:
950 10.1038/s41564-020-00813-8.

952 57. Long QX, Liu BZ, Deng HJ, Wu GC, Deng K, Chen YK, et al. Antibody
953 responses to SARS-CoV-2 in patients with COVID-19. *Nat Med.* 2020;26(6):845-8.
954 Epub 2020/05/01. doi: 10.1038/s41591-020-0897-1. PubMed PMID: 32350462.

955 58. Long QX, Tang XJ, Shi QL, Li Q, Deng HJ, Yuan J, et al. Clinical and

956 immunological assessment of asymptomatic SARS-CoV-2 infections. *Nat Med.* 2020.
957 Epub 2020/06/20. doi: 10.1038/s41591-020-0965-6. PubMed PMID: 32555424.

958 59. Sekizuka T, Itokawa K, Hashino M, Kawano-Sugaya T, Tanaka R, Yatsu K,
959 et al. A genome epidemiological study of SARS-CoV-2 introduction into Japan.
960 medRxiv. 2020:2020.07.01.20143958. doi: 10.1101/2020.07.01.20143958.

961 60. Koyama T, Platt D, Parida L. Variant analysis of SARS-CoV-2 genomes. *Bull
962 World Health Organ.* 2020;98(7):495-504. Epub 2020/08/04. doi:
963 10.2471/BLT.20.253591. PubMed PMID: 32742035; PubMed Central PMCID:
964 PMCPMC7375210.

965 61. Rouchka EC, Chariker JH, Chung D. Variant analysis of 1,040 SARS-CoV-2
966 genomes. *PLoS One.* 2020;15(11):e0241535. Epub 2020/11/06. doi:
967 10.1371/journal.pone.0241535. PubMed PMID: 33152019; PubMed Central PMCID:
968 PMCPMC7643988.

969 62. Matsuyama S, Nao N, Shirato K, Kawase M, Saito S, Takayama I, et al.
970 Enhanced isolation of SARS-CoV-2 by TMPRSS2-expressing cells. *Proc Natl Acad Sci
971 U S A.* 2020;117(13):7001-3. Epub 2020/03/14. doi: 10.1073/pnas.2002589117.
972 PubMed PMID: 32165541; PubMed Central PMCID: PMCPMC7132130.

973 63. Itokawa K, Sekizuka T, Hashino M, Tanaka R, Kuroda M. Disentangling
974 primer interactions improves SARS-CoV-2 genome sequencing by multiplex tiling
975 PCR. *PLoS One.* 2020;15(9):e0239403. Epub 2020/09/19. doi:
976 10.1371/journal.pone.0239403. PubMed PMID: 32946527; PubMed Central PMCID:
977 PMCPMC7500614.

978 64. Li H, Durbin R. Fast and accurate short read alignment with
979 Burrows-Wheeler transform. *Bioinformatics.* 2009;25(14):1754-60. Epub 2009/05/20.
980 doi: 10.1093/bioinformatics/btp324. PubMed PMID: 19451168; PubMed Central
981 PMCID: PMCPMC2705234.

982 65. Coil D, Jospin G, Darling AE. A5-miseq: an updated pipeline to assemble
983 microbial genomes from Illumina MiSeq data. *Bioinformatics.* 2015;31(4):587-9. Epub
984 2014/10/24. doi: 10.1093/bioinformatics/btu661. PubMed PMID: 25338718.

985 66. Shirato K, Nao N, Katano H, Takayama I, Saito S, Kato F, et al. Development
986 of Genetic Diagnostic Methods for Novel Coronavirus 2019 (nCoV-2019) in Japan. *Jpn
987 J Infect Dis.* 2020. Epub 2020/02/20. doi: 10.7883/yoken.JJID.2020.061. PubMed
988 PMID: 32074516.

989 67. Babraham AS. Bioinformatics - FastQC A Quality Control tool for High
990 Throughput Sequence Data [cited 24 Sep 2020]. Available from:
991 <https://www.bioinformatics.babraham.ac.uk/projects/fastqc/>.

992 68. Bolger AM, Lohse M, Usadel B. Trimmomatic: a flexible trimmer for
993 Illumina sequence data. *Bioinformatics*. 2014;30(15):2114-20. Epub 2014/04/04. doi:
994 10.1093/bioinformatics/btu170. PubMed PMID: 24695404; PubMed Central PMCID:
995 PMCPMC4103590.

996 69. Dobin A, Davis CA, Schlesinger F, Drenkow J, Zaleski C, Jha S, et al. STAR:
997 ultrafast universal RNA-seq aligner. *Bioinformatics*. 2013;29(1):15-21. Epub
998 2012/10/30. doi: 10.1093/bioinformatics/bts635. PubMed PMID: 23104886; PubMed
999 Central PMCID: PMCPMC3530905.

1000 70. Liao Y, Smyth GK, Shi W. featureCounts: an efficient general purpose
1001 program for assigning sequence reads to genomic features. *Bioinformatics*.
1002 2014;30(7):923-30. Epub 2013/11/15. doi: 10.1093/bioinformatics/btt656. PubMed
1003 PMID: 24227677.

1004 71. Anders S, Huber W. Differential expression analysis for sequence count data.
1005 *Genome Biol.* 2010;11(10):R106. Epub 2010/10/29. doi: 10.1186/gb-2010-11-10-r106.
1006 PubMed PMID: 20979621; PubMed Central PMCID: PMCPMC3218662.

1007 72. CRAN. Package pheatmap [cited 24 Sep 2020]. Available from:
1008 <https://cran.r-project.org/web/packages/pheatmap/index.html>.

1009 73. Weiner 3rd J DT. tmod: an R package for general and multivariate enrichment
1010 analysis. *PeerJ Preprints*. 2016. doi: 10.7287/peerj.preprints.2420v1.

1011 74. Smyth GK. limma: Linear Models for Microarray Data. In: Gentleman R.
1012 CVJ, Huber W., Irizarry R.A., Dudoit S., editor. *Bioinformatics and Computational
1013 Biology Solutions Using R and Bioconductor* Springer, New York, NY: Springer, New
1014 York, NY; 2005. p. 397-420.

1015

1016

1017 **Data availability**

1018 All relevant data are provided in the manuscript and the Supporting Information files.

1019

1020 **Funding**

1021 N.N. was funded through the Research Program on Emerging and Reemerging Infectious
1022 Diseases from the Japan Agency for Medical Research and Development (JP19fk0108072) and
1023 by a grant-in-aid for scientific research from the Ministry of Education, Culture, Sports,
1024 Science, and Technology in Japan (18H02665). H.S. was funded through the Japan Agency for
1025 Medical Research and Development (JP19fk0108084). T. Su was funded through the Japan
1026 Agency for Medical Research and Development (JP19fk0108104, JP20fk0108104, and
1027 JP19fk0108110). H.H. was funded through the Japan Agency for Medical Research and
1028 Development (JP19fk0108112). The funders played no role in study design, data collection and
1029 analysis, decision to publish, or preparation of the manuscript.

1030

1031 **Competing interests**

1032 The authors have declared no competing interests.

1033

1034 **Author contributions**

1035 Conceptualization: NN, NI-Y, T. Su, HH

1036 Data Curation: NN

1037 Formal Analysis: NN, KS, AA

1038 Funding Acquisition, NN, HS, T. Su, HH

1039 Investigation: NN, NI-Y, KS, AA, NS, MS, NK, TA, YS, TH, YK, YA, SI, HK, SF, T. Se, T.
1040 Su
1041 Methodology: NN, NI-Y, KS, AA, YA, T. Su
1042 Project Administration: NN, T. Su, HH
1043 Resources: NN, NI-Y, KS, AA, HS, T. Su, HH
1044 Supervision: NN, T. Su, HH
1045 Validation: NN, T. Su, HH
1046 Visualization: NN, KS
1047 Writing - Original Draft: NN, KS
1048 Writing - Review & editing: NN, NI-Y, KS, AA, NS, MS, NK, TA, YS, TH, YK, YA, SI, HK,
1049 SF, T. Se, HS, T. Su, and HH
1050

1051 **Figure legends**

1052

1053 **Fig. 1. Study design and clinical scores in cynomolgus monkeys after inoculation of**

1054 **SARS-CoV-2.** Study outline (A). Black arrows indicate preparation for experimental

1055 infection. Six 5-year-old monkeys were selected from 25 monkeys. Red and yellow arrow heads

1056 indicate virus inoculation. After assigning animals to "CD3+ high" and "CD3+ low" groups, six

1057 cynomolgus monkeys were infected with an isolate from East Asia (WK-521 strain) via a

1058 combination of intranasal (0.125 mL, sprayed into the right nostril), conjunctival (0.1 mL,

1059 dropped into the right eye), and intratracheal (1.275 mL virus solution plus 2 mL saline via a

1060 catheter) inoculation. After the initial inoculation, body weight was measured, and samples were

1061 collected at various time points (blue arrows). Red arrows denote autopsy at 7 or 14 days after

1062 the first or second inoculation (n = 1 per group at each time point). Four monkeys received a

1063 second inoculation with an isolate from Europe (QH-329-037 strain). (B) Clinical scores of

1064 cynomolgus monkeys inoculated with SARS-CoV-2. Cool (blue and aqua) and warm (red and

1065 orange) colored symbols and lines indicate data from the CD3+ high group and CD3+ low

1066 group animals, respectively. After transfer to the ABSL3 facility, the monkeys were observed

1067 once daily for clinical signs and scored accordingly. Black dashed lines on the horizontal axis

1068 indicate the range of clinical scores recorded during the ABSL3 facility acclimatization period.

1069 Each dot/line represents data from an individual animal after initial inoculation with

1070 SARS-CoV2. The brown dashed line on the vertical axis indicates the day of the second

1071 inoculation.

1072

1073

1074 **Fig. 2. Hematological examination of cynomolgus monkeys inoculated with**
1075 **SARS-CoV-2.** Hemoglobin (HGB) in EDTA-treated whole blood samples was examined at
1076 various time points after inoculation (A). Absolute numbers of lymphocytes and monocytes in
1077 EDTA-treated whole blood samples were determined at various time points after inoculation
1078 (B). Leukocyte differentiation (e.g., CD3, CD20, and CD16) at various time points after
1079 inoculation was examined by flow cytometry (C). Cytokine and chemokine levels in serum
1080 from each cynomolgus monkey inoculated with SARS-CoV-2 (D). Representative cytokines
1081 were profiled by multiplex analysis. Assays were performed using unicate samples at each time
1082 point. Cool (blue and aqua) and warm (red and orange) colored symbols and lines indicate data
1083 from the CD3+ high and CD3+ low groups, respectively. Each dot/line represents data from an
1084 individual animal. The brown dashed line on the vertical axis indicates the day of the second
1085 inoculation.

1086

1087 **Fig. 3. Detection of virus excretion in clinical samples from cynomolgus monkeys**
1088 **inoculated with SARS-CoV-2.** Six cynomolgus monkeys were used in this study. Cool
1089 (blue and aqua) and warm (red and orange) colored bars indicate data from CD3+ high and
1090 CD3+ low groups, respectively. Each bar represents data from an individual animal. After initial
1091 viral inoculation with the WK-521 strain, clinical samples (conjunctiva, nasal, throat, and rectal
1092 swabs) were collected. The second inoculation with QH-329-037 strain was performed 35 days
1093 after the first inoculation. + indicates samples that were positive for subgenomic mRNA (black)
1094 or virus (red). The brown dashed line on the vertical axis indicates the day of the second

1095 inoculation.

1096

1097

1098 **Fig. 4. Seroconversion after SARS-CoV-2 inoculation.** Neutralizing antibody titers
1099 (against the WK-521 strain) in sera (A). Antibody subclasses and specificity for the spike (S),
1100 receptor binding domain (RBD), and nucleocapsid (N) proteins were assessed using in-house
1101 IgM, IgA, and IgG ELISAs (B). Cool (blue and aqua) and warm (red and orange) colored
1102 symbols and lines indicate data from the CD3+ high and CD3+ low groups, respectively. Each
1103 dot/line represents data from an individual animal. R, correlation coefficient (Spearman's
1104 correlation analysis) between the neutralization and ELISA tests. The brown dashed line on the
1105 vertical axis indicates the day of the second inoculation.

1106

1107 **Fig. 5. Transcriptome analysis of blood samples obtained after SARS-CoV-2**
1108 **inoculation.** Gene set enrichment analysis was performed on samples from the CD3+ high
1109 group and CD3+ low group samples after (Days 1, 4, 7, R0, R1, R4, and R7) virus infection
1110 (A). The name of each significantly enriched module is listed, along with the module ID (in
1111 brackets) ($P < 0.01$). Green and gray dots indicate inflammation- and B cell response-related
1112 modules, respectively. Red and blue indicate the proportion of genes in a particular module that
1113 is upregulated or downregulated in the CD3+ high group compared with the CD3+ low group.
1114 Each module is represented by a box, where the width is proportional to the effect size
1115 (AUROC value calculated from the number of genes in the module and ranking by the Cerny
1116 test), while brighter colors indicate lower P -values. Gene set enrichment analysis in the CD3+

1117 high group (left panel) and CD3+ low group (right panel) at different time points after virus
1118 infection (Days 1, 4, 7, R0, R1, R4, and R7) compared with baseline (before virus infection:
1119 Day 0) (B). The name of each significantly enriched module name is listed along with module
1120 ID (in brackets) ($P < 0.01$). Yellow, green & red, gray, and black dots indicate modules related
1121 to innate immunity, inflammation, CD4+ T cell response, and T & NK cell responses,
1122 respectively. Red and blue indicate the proportion of genes in a particular module that is
1123 upregulated or downregulated in the CD3+ high group compared with the CD3+ low group.
1124 Each module is represented as a pie chart, where the size is proportional to the effect size
1125 (AUROC value calculated from the number of genes in the module and ranking by the Cerny
1126 test), while brighter colors indicate lower P -values.

1127

1128 **Fig. 6. Detection of virus RNA in tissue samples from cynomolgus monkeys**
1129 **inoculated with SARS-CoV-2.** Tissue samples were obtained from monkeys at 7 days
1130 post-inoculation with WK-521 strain (#5404 and #5417), and at 7 days (#5403 and #5412) or 14
1131 days (#5399 and #5405) after re-infection with QH-329-037 strain. Cool (blue and aqua) and
1132 warm (red and orange) colored bars indicate data from the CD3+ high group and CD3+ low
1133 group, respectively. Each bar represents data from an individual animal.

1134

1135 **Fig. 7. Pathology of cynomolgus monkeys inoculated with SARS-CoV-2.** (A) Gross
1136 pathology of lungs from monkeys at 7 days post-inoculation with WK-521 strain (#5404 and
1137 #5417), and at 7 days (#5403 and #5412) or 14 days (#5399 and #5405) after re-infection with
1138 QH-329-037 strain. Ischemic changes and consolidation were observed in the lower lobe of the

1139 right lung of monkey #5417 (red arrows). Other lobes showed congestion and collapse (white
1140 arrows). Yellow arrows indicate swollen lung lymph nodes in monkeys #5403, #5412, and
1141 #5399. Atrophic changes are seen in the pulmonary margin in monkeys #5412 and #5405 (blue
1142 arrows). (B) Representative histopathology of lungs from monkeys at 7 days post-inoculation
1143 with WK-521 strain (#5404 and #5417). Collections of mononuclear cells were seen in the
1144 airspaces of the middle lobe of the right lung of monkey #5404 (B, upper row). Pulmonary
1145 edema with polymorphonuclear leukocyte infiltration and proliferating type II cells overlying
1146 pulmonary walls were observed in the lower lobe of the right lung of monkey #5417 (B, lower
1147 row). Scale bars: 500 μ m (left column), 50 μ m (middle column), and 20 μ m (right column).
1148 Hematoxylin and eosin staining (H&E). (C) Double immunohistochemistry identified cell
1149 collections in alveolar air spaces at 7 days after the initial inoculation (upper row from #5404;
1150 lower row from #5417). Infiltrating cells were CD68+ (brown) or CD3+ (green). Bars in C, 50
1151 μ m (left) and 20 μ m (right). An anti-CD68 rabbit polyclonal antibody (brown) and an
1152 anti-CD3-monoclonal antibody (green) were used for IHC in C.

1153

1154 **Supporting information**

1155 **S1 Fig. Selection of monkeys for experimental infection.** (A) Body weight of the 25
1156 monkeys in Figure 1. (B) Analysis of lymphocytes in peripheral blood from 15 animals
1157 weighing <3.4 kg. Each dot represents data from an individual animal. The blue and red colored
1158 symbols denote data from the CD3+ high and low groups, respectively.

1159

1160 **S2 Fig. Clinical course in cynomolgus monkeys inoculated with SARS-CoV-2.** Body

1161 weight was measured under anesthesia at various time points after inoculation (A). Biochemical
1162 markers including globulin (Glob), albumin (ALB), glucose, alkaline phosphatase (ALP), and
1163 blood urea nitrogen (BUN) in lithium-heparin treated whole blood samples were measured at
1164 various time points after inoculation (B). Six cynomolgus monkeys were used. Cool (blue and
1165 aqua) and warm (red and orange) colored symbols and lines indicate data from the CD3+ high
1166 and CD3+ low groups, respectively. Each dot/line represents data from an individual animal.
1167 The brown dashed line on the vertical axis indicates the day of second inoculation.

1168

1169 **S3 Fig. Variations in deep body temperature detected by the temperature logger.**
1170 Thermo logger probes were set intraperitoneally at 14 days before inoculation. Black arrows,
1171 animal transfer date (under anesthesia) from the animal facility to the animal biosafety level 3
1172 (ABSL3); red and yellow arrow heads, virus inoculation under anesthesia with a mixture of
1173 ketamine and xylazine; Red brace, deviation from diurnal variation indicates high fever. The
1174 fluctuation of deep body temperature within a day was maintained during ABSL3
1175 acclimatization. A drop in deep body temperature due to the mixed anesthesia was observed on
1176 the day of inoculation.

1177

1178 **S4 Fig. Hematological examination of cynomolgus monkeys inoculated with**
1179 **SARS-CoV-2.** Erythrocyte analysis, including total red blood cells (RBC) and hematocrit
1180 (HCT), was performed using EDTA-treated whole blood samples taken at various time points
1181 after inoculation (A). Absolute white blood cell (WBC) count, including total WBC,
1182 neutrophils, eosinophils, and basophils, in EDTA-treated whole blood samples was measured at

1183 various time points after inoculation (B). Markers of leukocyte differentiation, CD4 and CD8,
1184 were detected by flow cytometry at various time points after inoculation (C). Cool (blue and
1185 aqua) and warm (red and orange) colored symbols and lines indicate data from the CD3+ high
1186 and CD3+ low groups, respectively. Each dot/line represents data from an individual animal.
1187 The brown dashed line on the vertical axis indicates the day of the second inoculation.

1188

1189 **S5 Fig. Cytokine and chemokine levels in serum samples from cynomolgus**
1190 **monkeys inoculated with SARS-CoV-2.** Sera were obtained from six monkeys at various
1191 time points after inoculation. Pro-inflammatory cytokines and chemokines (A), helper T
1192 cell-related cytokines (B), and other representative factors in serum that drive proliferation of
1193 epithelial cells (TGF- α) and neutrophils (IL-8) (C) were profiled by multiplex analysis. Assays
1194 were performed using unicate samples per time point. Cool (blue and aqua) and warm (red and
1195 orange) colored symbols and lines indicate data from the CD3+ high and CD3+ low groups,
1196 respectively. Each dot/line represents data from an individual animal. The brown dashed line on
1197 the vertical axis indicates the day of the second inoculation.

1198

1199 **S6 Fig. Detection of subgenomic RNA in clinical samples and tissue samples from**
1200 **cynomolgus monkeys inoculated with SARS-CoV-2.** Virus RNA-positive samples from
1201 Figures 3 and 6 were re-examined to detect viral RNA and subgenomic RNA using three primer
1202 sets (A and B, respectively).

1203

1204 **S7 Fig. Transcriptome analysis of blood samples from cynomolgus monkeys**

1205 **inoculated with SARS-CoV-2.** Volcano plot showing the magnitude and significance of
1206 differentially expressed genes between samples collected from animals before (Day 0) and after
1207 (Days 1, 4, 7, R0, R1, R4, and R7) virus infection (A). Red plots indicate genes that were
1208 upregulated significantly (331 genes) after virus infection, and blue plots indicate genes that
1209 were downregulated significantly (176 genes) after virus infection (adjusted *P*-value < 0.05).
1210 Plots shown in brighter red or blue represent genes that were either upregulated (190/331 genes)
1211 or downregulated (86/176 genes) by more than 2-fold. Expression of immunity-related genes in
1212 peripheral whole blood samples collected from animals before (Day 0) and after (Days 1, 4, 7,
1213 R0, R1, R4, and R7) virus infection (B). Heatmaps showing normalized counts per gene, scaled
1214 by rows of 78 immune-related genes among the 507 genes significantly upregulated or
1215 downregulated by virus infection (adjusted *P*-value < 0.05). Gene symbols are listed on the
1216 right. Yellow and green/red dots indicate genes related to innate immunity and inflammation,
1217 respectively. Each column represents a different sample. Animal ID, days post-virus infection
1218 (dpi), and CD3+ expression in each sample are shown at the top.

1219

1220 **S8 Fig. Double immunohistochemistry to detect virus antigens (brown) and ACE2**
1221 **(green) in the lungs at 7 days after initial inoculation.** ACE2 was detected in the intact
1222 brush border of the respiratory epithelia in the intrapulmonary bronchus (black arrows);
1223 however, no cells were positive for viral antigens (red arrow; upper row, left). Viral antigen was
1224 detected in linear pneumocytes and type I pneumocytes (red arrow), and slight expression of
1225 ACE2 was detected in round pneumocytes (suggestive of type II pneumocytes) (black arrows),
1226 in the alveolar area in the absence of inflammatory infiltration (upper row, right). Strong

1227 expression of ACE2 on large pneumocytes suggested hyperplasia of type II pneumocytes (black
1228 arrows, lower row); there were no degenerated viral antigen-positive pneumocytes (red arrow,
1229 lower row, left) at the lesion sites in the alveolar area. Bars, 20 μ m. An anti-SARS-CoV-2
1230 nucleocapsid protein rabbit polyclonal antibody and an anti-ACE2 goat-polyclonal antibody
1231 were used for IHC.

1232

1233 **S9 Fig. Lung pathology in cynomolgus monkeys receiving a second inoculation**
1234 **with SARS-CoV-2.** Representative histopathology images of lungs from monkeys obtained at
1235 7 days (#5403 and #5412) or 14 days (#5399 and #5405) after re-infection with QH-329-037
1236 strain. Cellular infiltration, including lymphocytes and macrophages, can be seen around the
1237 bronchi and in the alveoli in the middle lobe of the right lung from monkey #5403 (first row).
1238 Lymphoid aggregates, including alveolar macrophages, were observed in the alveoli in the
1239 upper lobe of the right lung from monkey #5399 (second row). Lymphoid aggregates around
1240 small vessels (red arrowheads) and fibrotic inflammation with lymphocyte aggregation in the
1241 alveolar area and pleura (blue arrowheads) were seen in the right lung from monkeys #5412 and
1242 #5405 (third and fourth rows). Scale bars: 500 μ m (left column), 50 μ m (middle column), and
1243 20 μ m (right column). Hematoxylin and eosin staining (H&E).

1244

1245 **S10 Fig. Representative images of histopathological lesions from cynomolgus**
1246 **monkeys after experimental inoculation with SARS-CoV-2.** Representative
1247 hemophagocytosis images of the lung and lymph nodes from monkey #5417 obtained at 7 days
1248 after infection with WK-521 strain (A). Hemophagocytes are seen in the alveoli and sinus of the

1249 cervical and splenic lymph nodes (yellow arrows). Scale bars: 50 μ m (left column) and 20 μ m
1250 (right column). Hematoxylin and eosin (H&E) staining. Eosinophil (yellow arrows) and plasma
1251 cell (blue arrows) infiltration into the mesenteric lymph node and intestines from monkey #5412
1252 at 7 days after the second inoculation with QH-329-037 (B). Cellular infiltration, including
1253 eosinophils and plasma cells, can be seen in the sinus of the mesenteric lymph node and the
1254 lamina propria of the small and large intestine. Scale bars: 500 μ m (left column) and 20 μ m
1255 (right column). H&E staining.

1256

1257

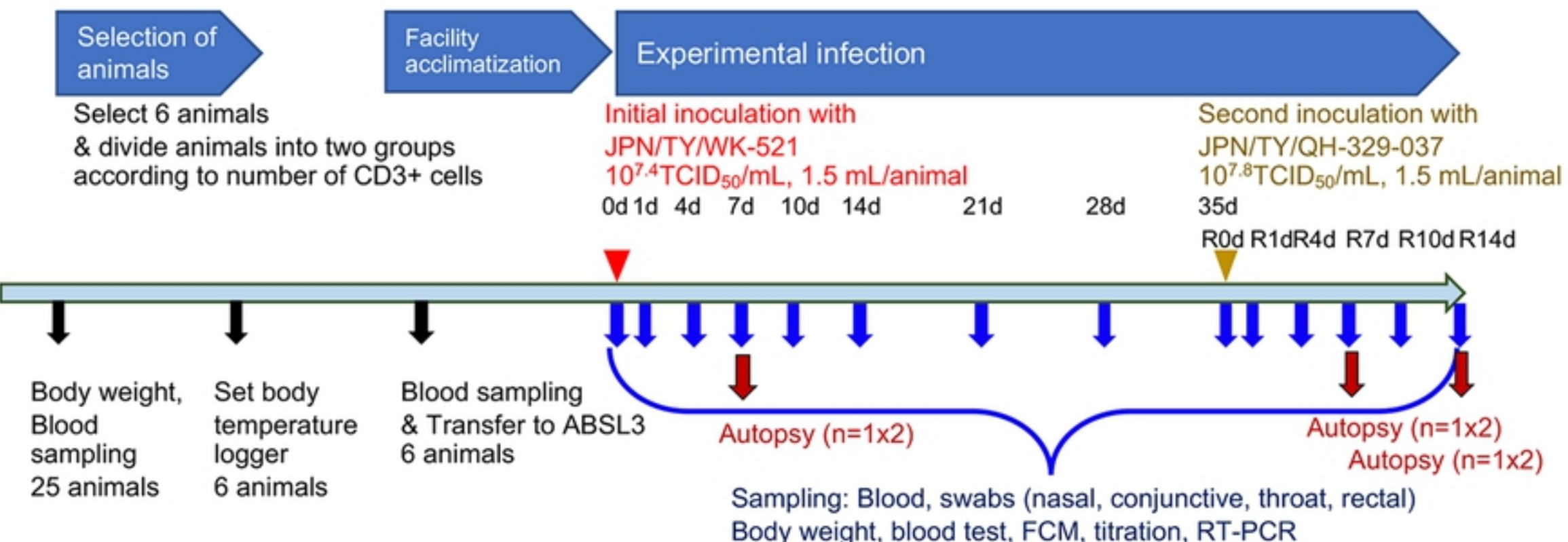
1258 **S1 Table. Cross neutralization of two strains of SARS-CoV-2 in monkey sera after**
1259 **experimental infection.**

1260 **S2 Table. Summary of the results of next generation sequencing of SARS-CoV-2**
1261 **from tissue samples of experimentally infected monkeys**

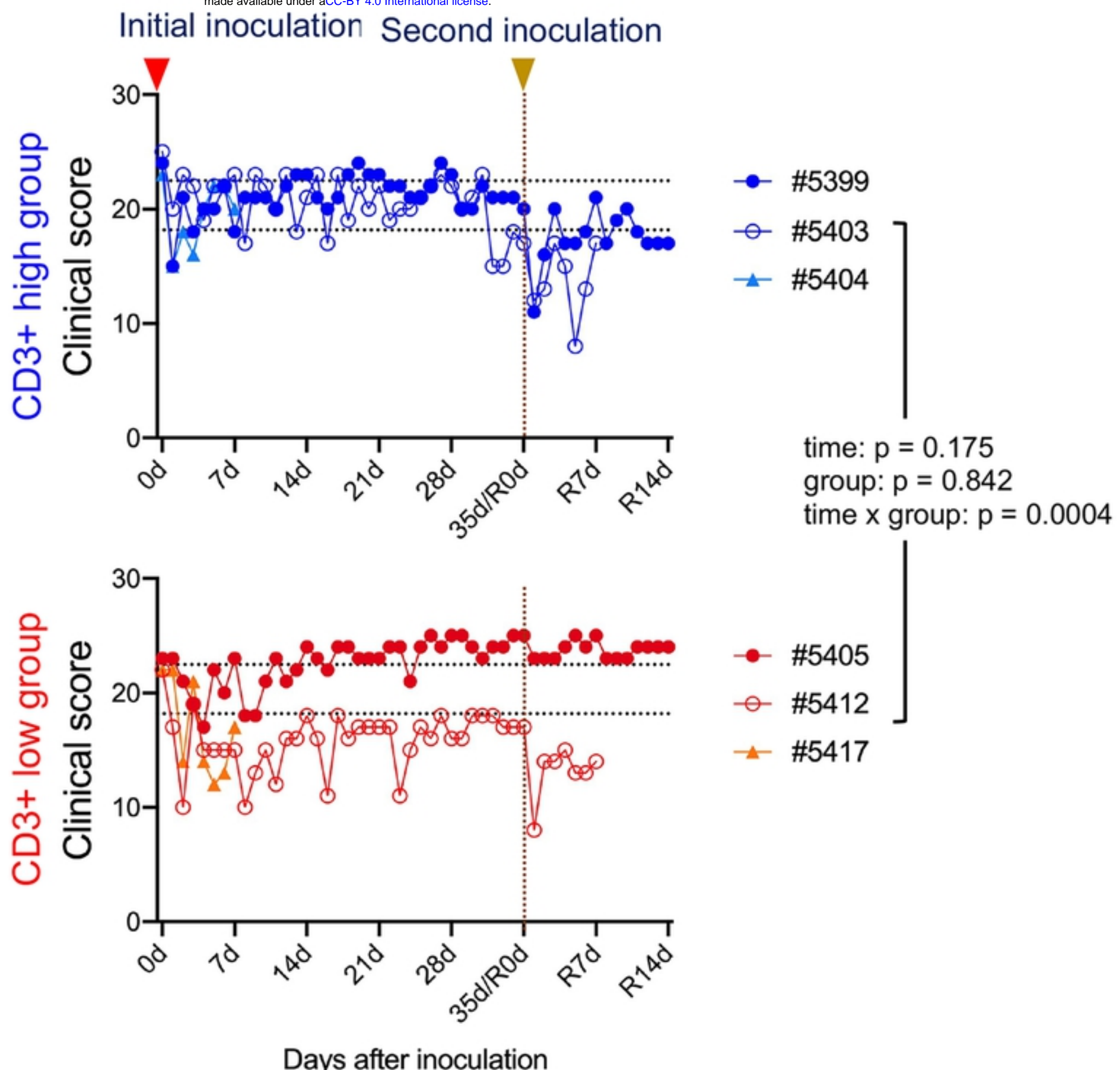
1262 **S3 Table. D614G variants in tissue samples from experimentally infected monkeys**

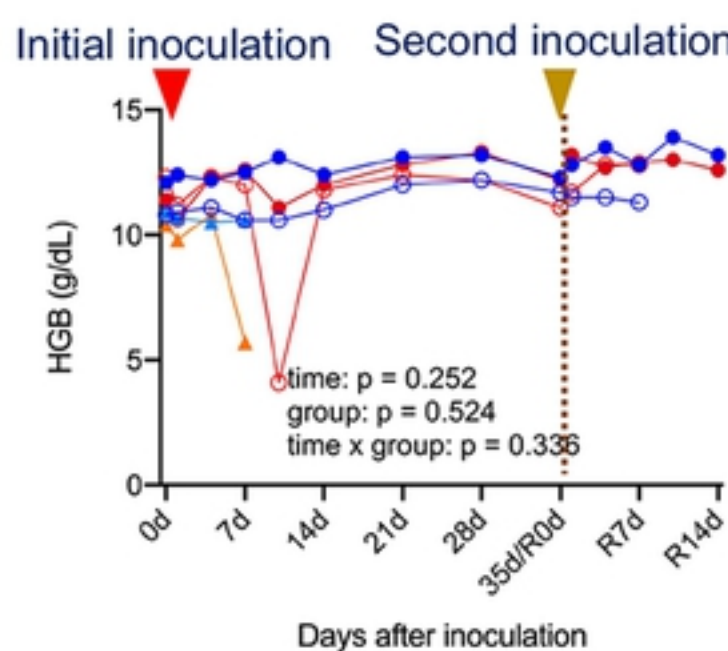
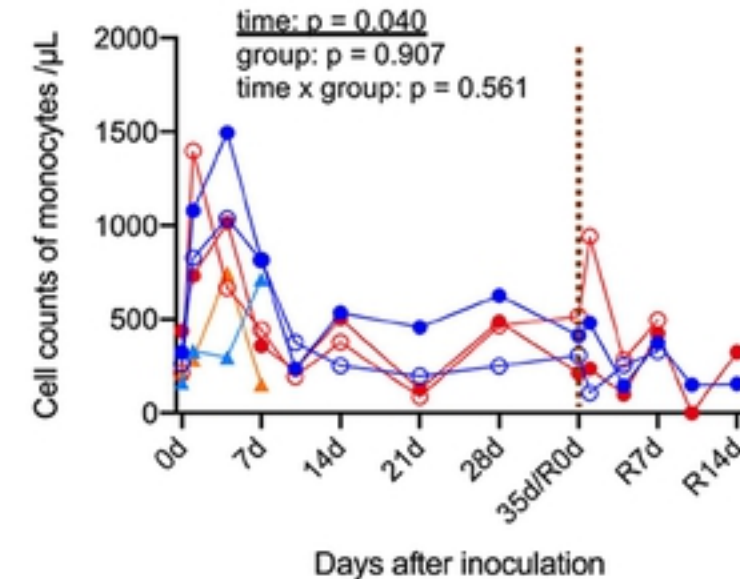
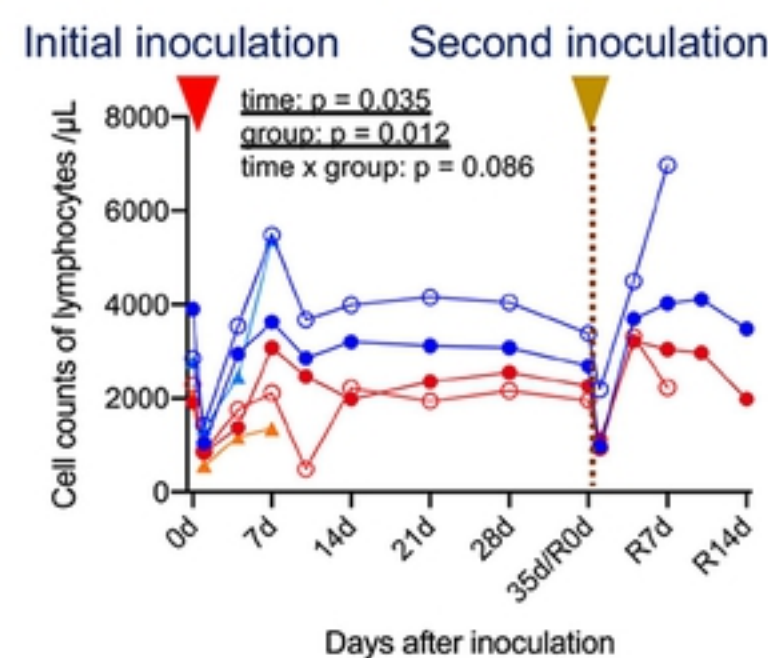
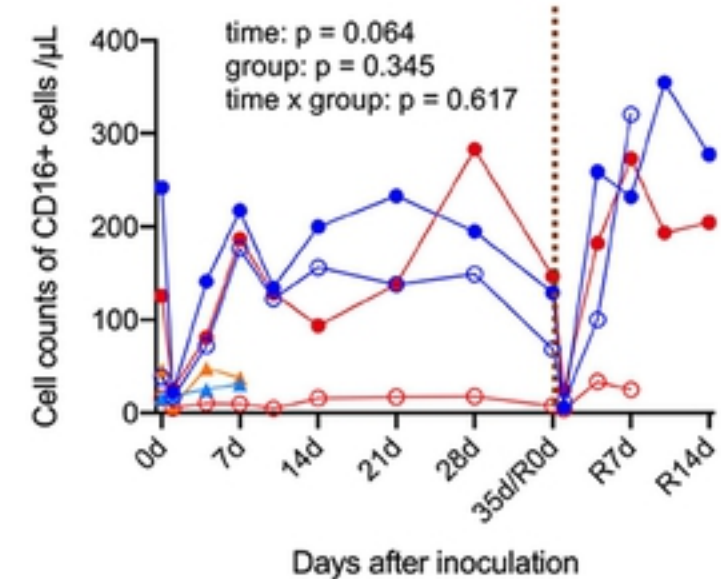
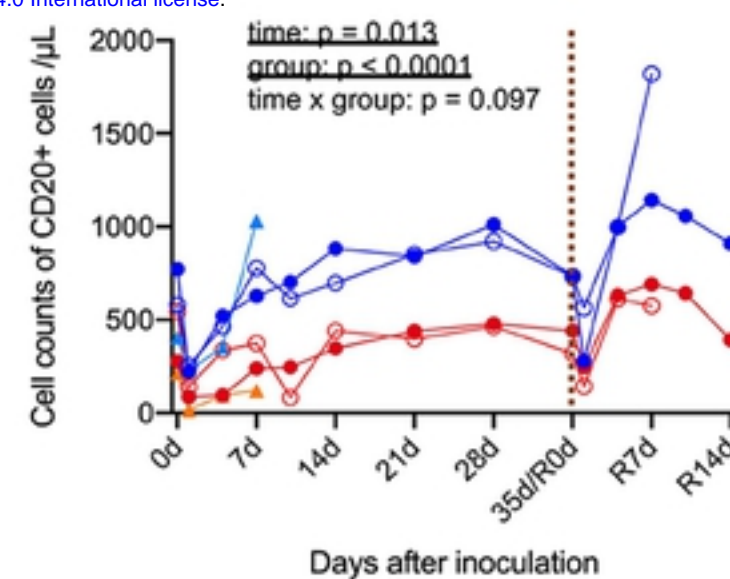
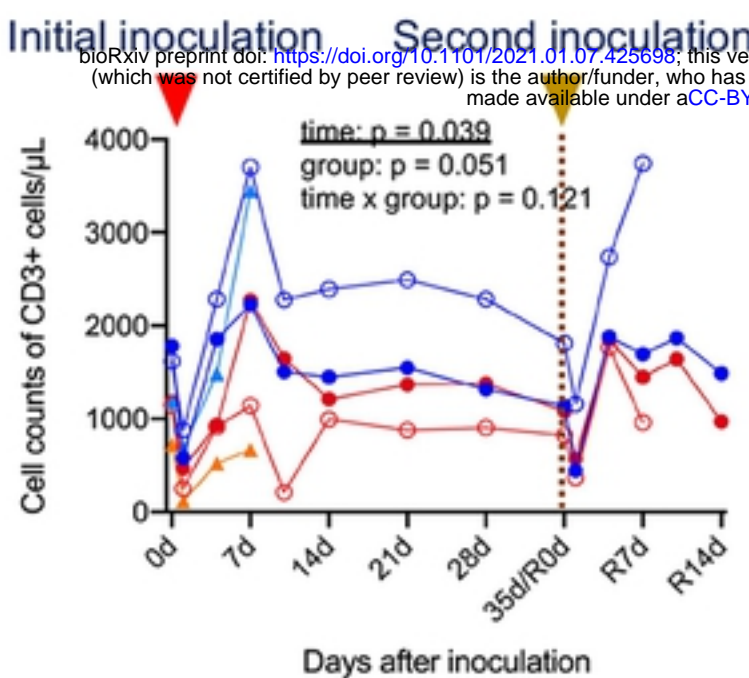
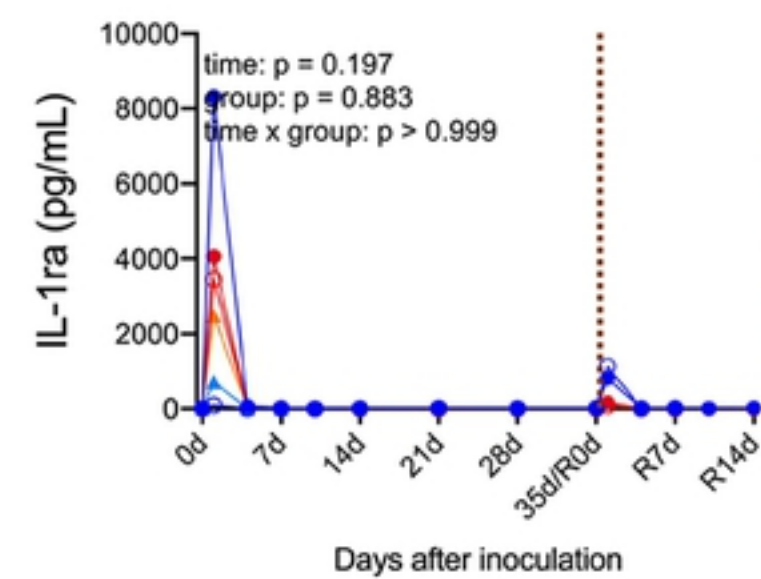
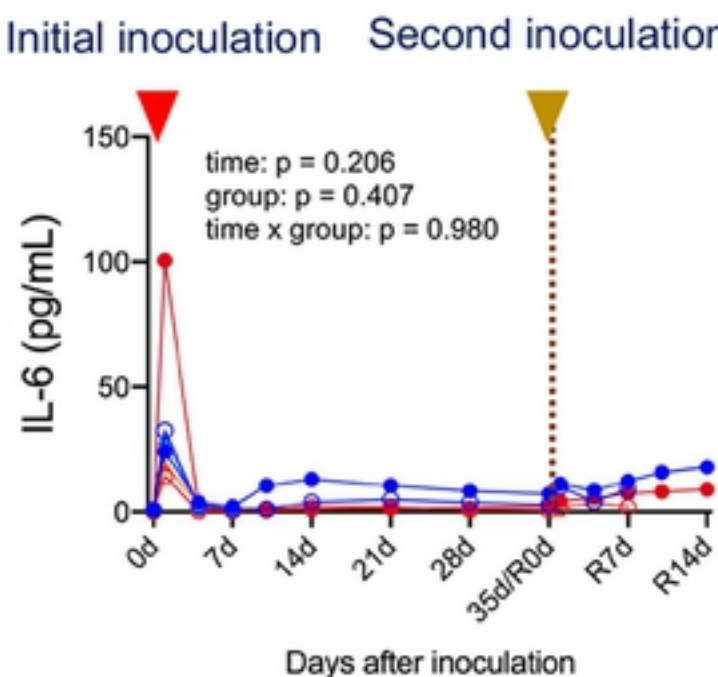
1263 **S4 Table. Primer and probe sets used in this study.**

1264

A

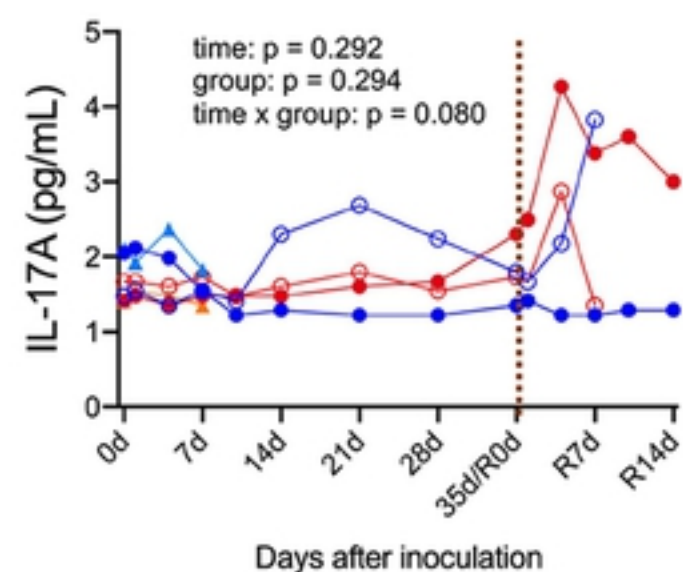
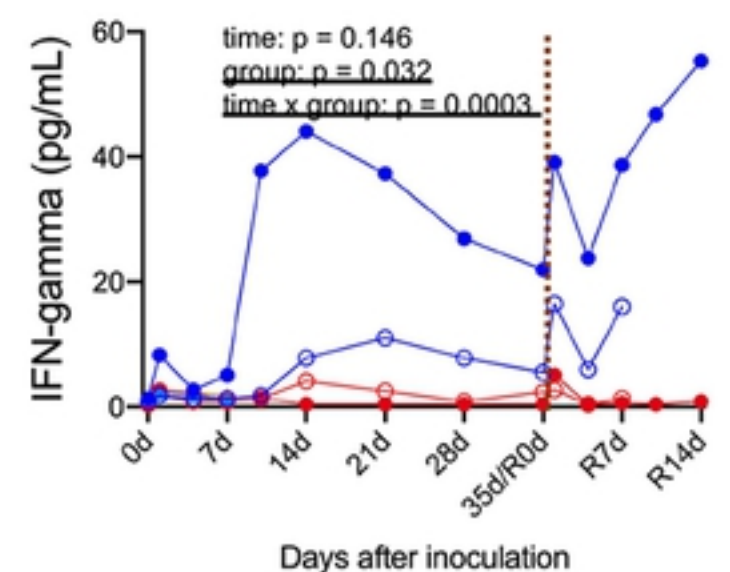
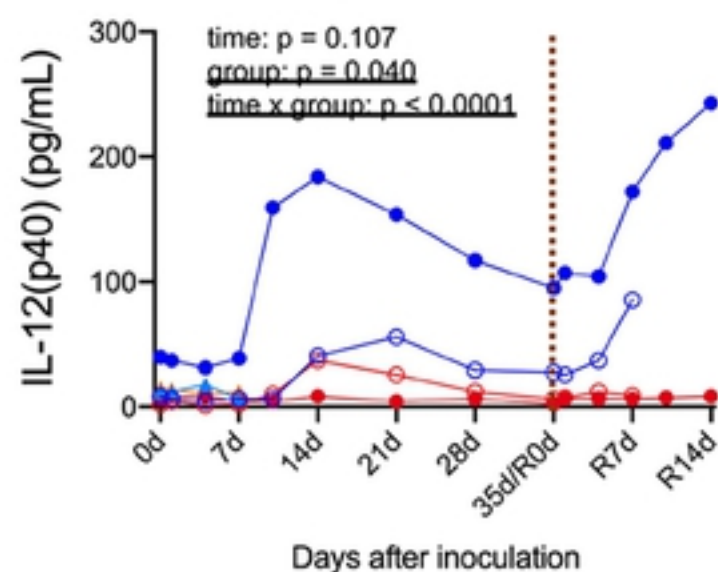
bioRxiv preprint doi: <https://doi.org/10.1101/2021.01.07.425698>; this version posted January 7, 2021. The copyright holder for this preprint (which was not certified by peer review) is the author/funder, who has granted bioRxiv a license to display the preprint in perpetuity. It is made available under aCC-BY 4.0 International license.

B**Figure 1**

A**B****C****D**

CD3+ high group
CD3+ low group

- #5399
- #5403
- △ #5404
- #5405
- #5412
- △ #5417

**Figure 2**

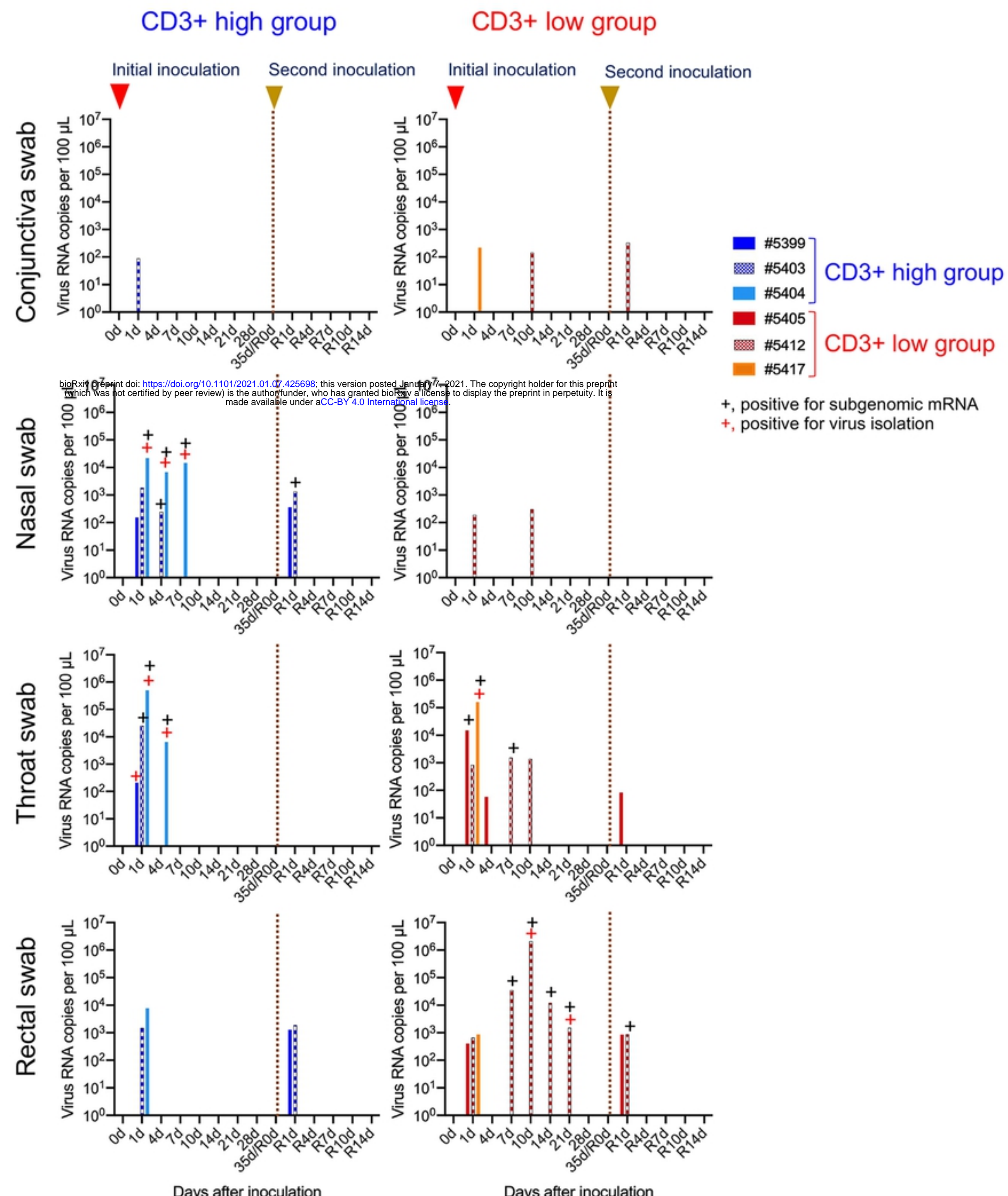
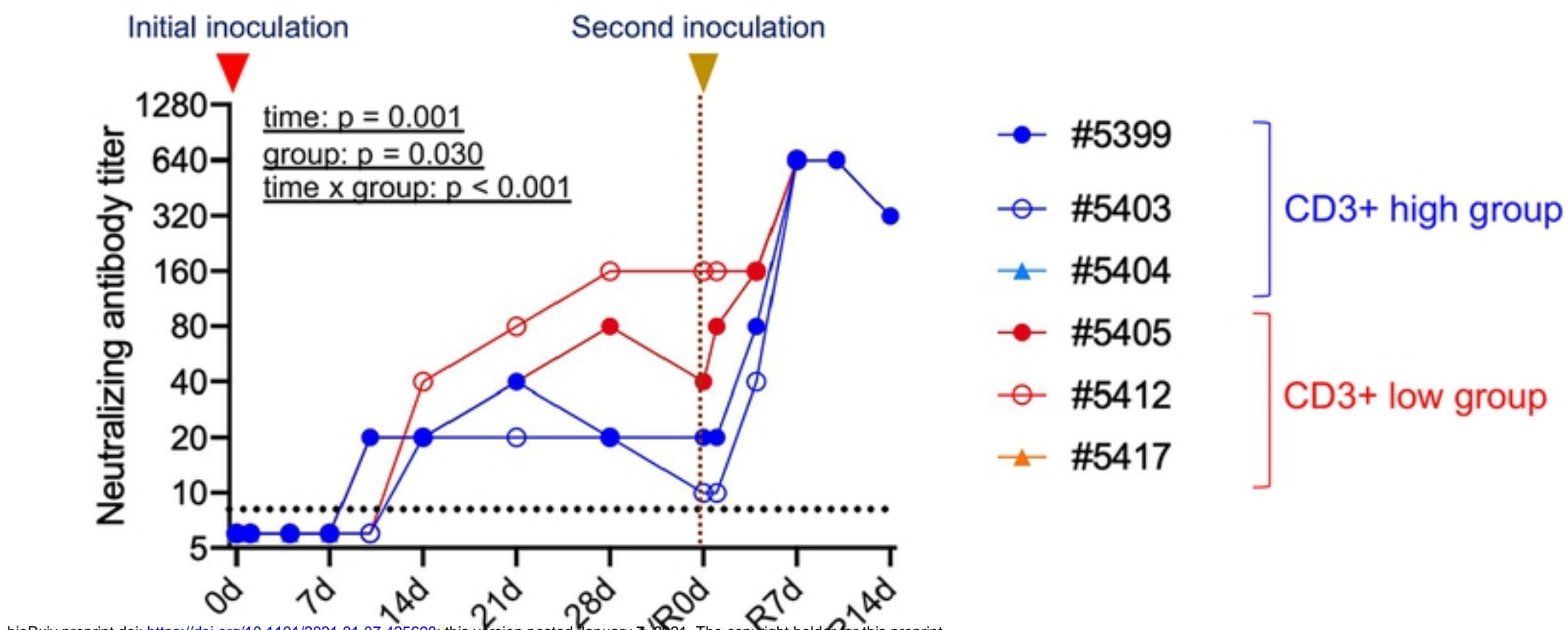


Figure 3

A



bioRxiv preprint doi: <https://doi.org/10.1101/2021.01.07.425698>; this version posted January 7, 2021. The copyright holder for this preprint (which was not certified by peer review) is the author/funder, who has granted bioRxiv a license to display the preprint in perpetuity. It is made available under aCC-BY 4.0 International license.

B

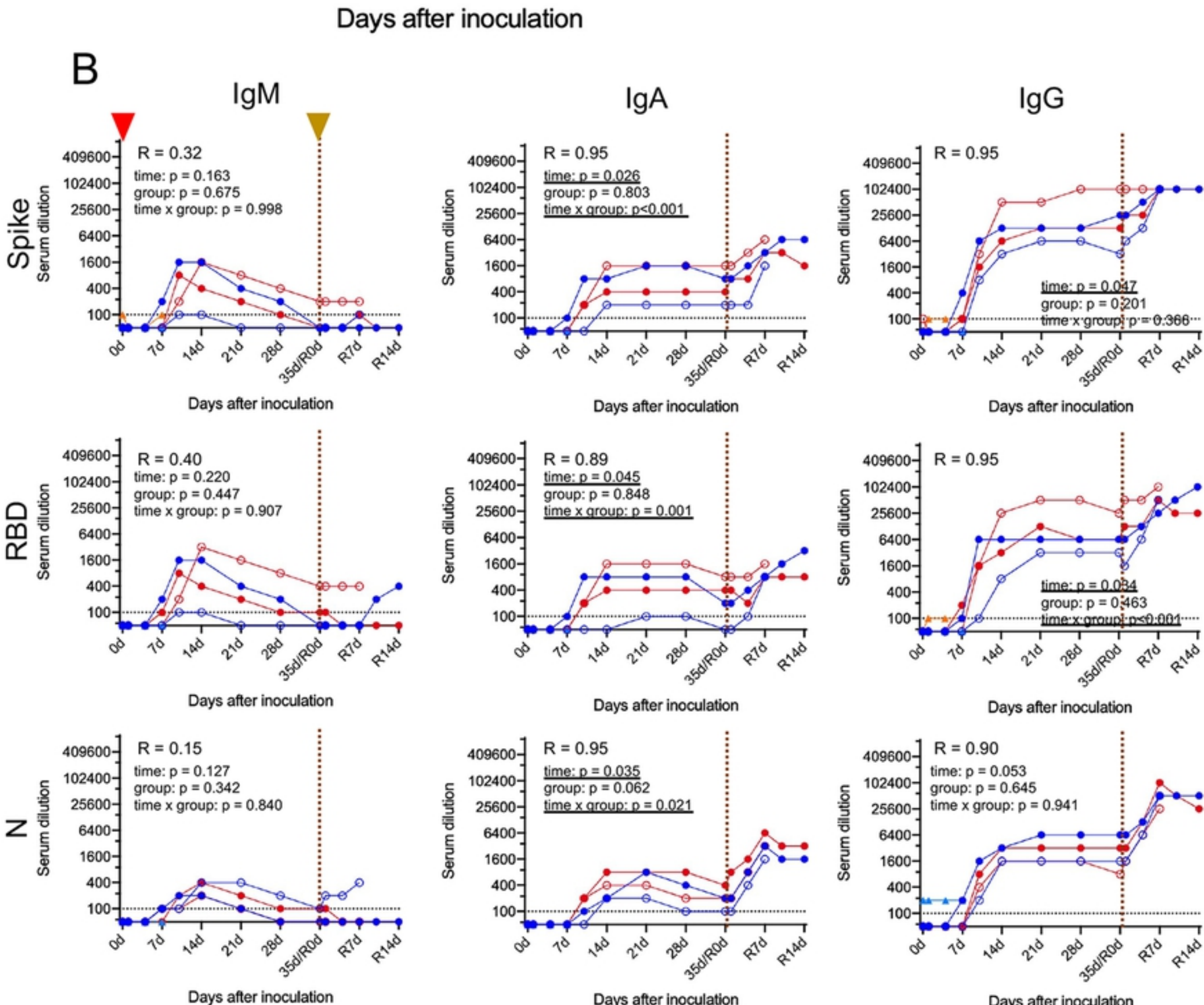
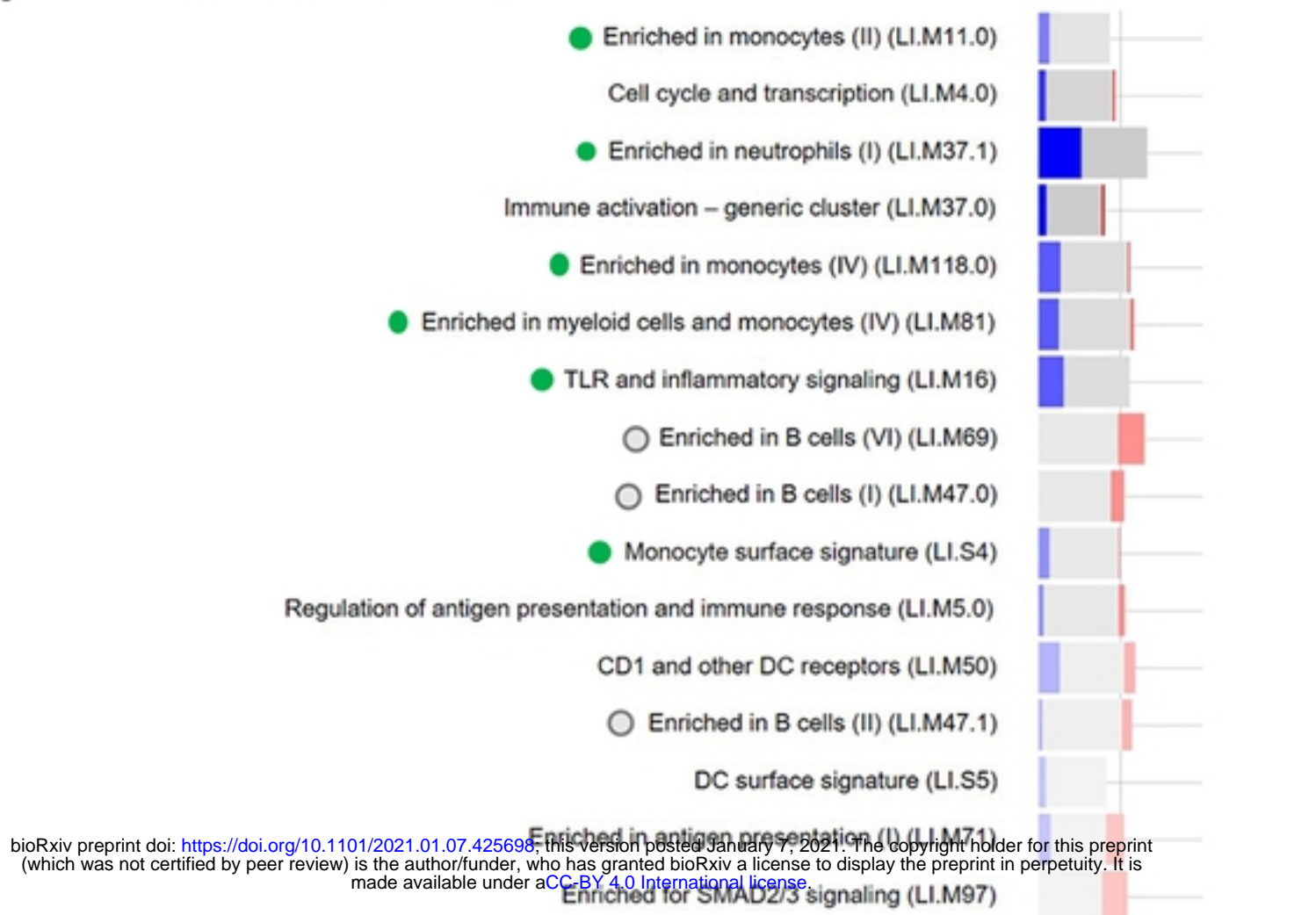


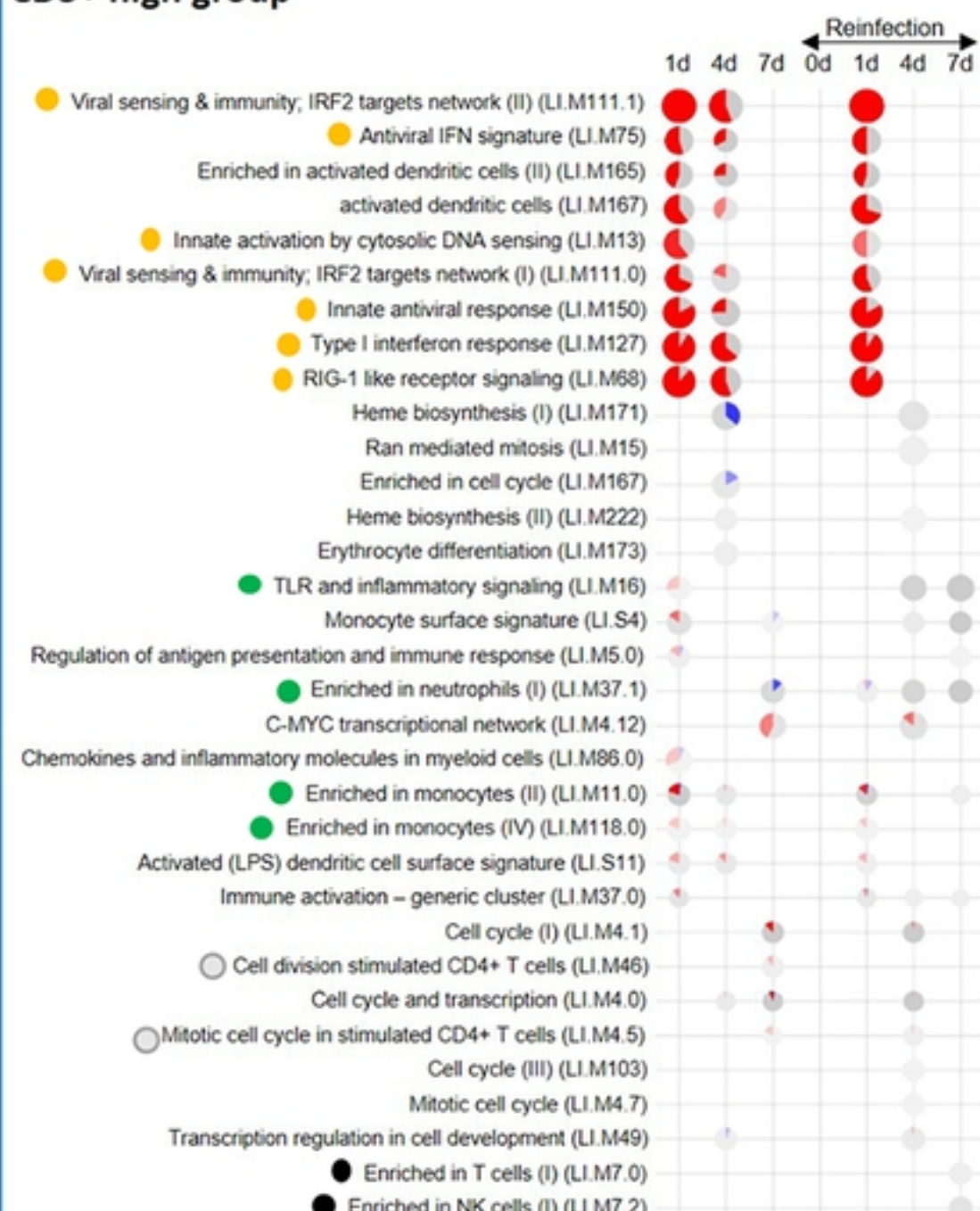
Figure 4

A CD3+ high vs CD3+ low group



B

CD3+ high group



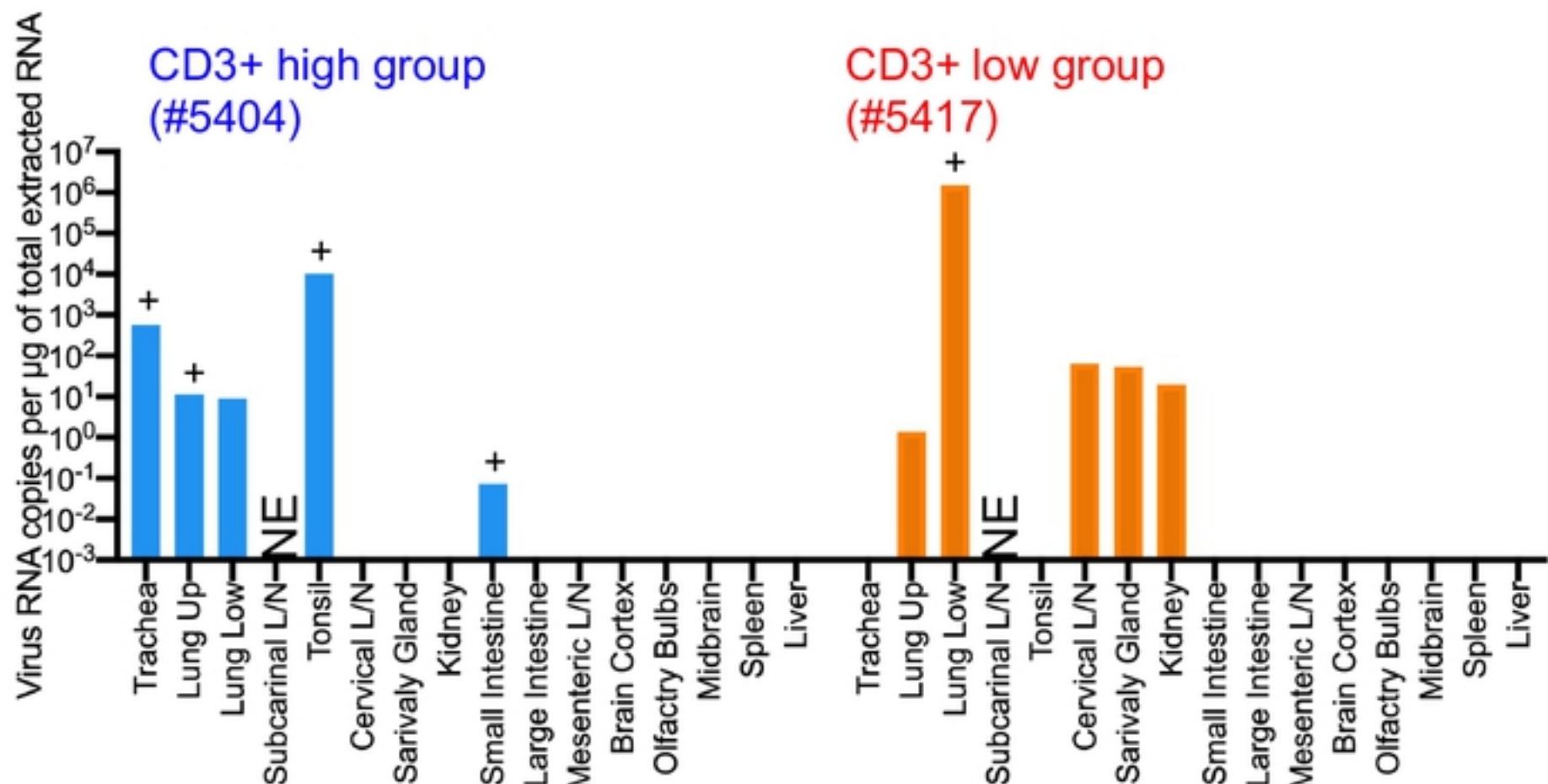
CD3+ low group



Figure 5

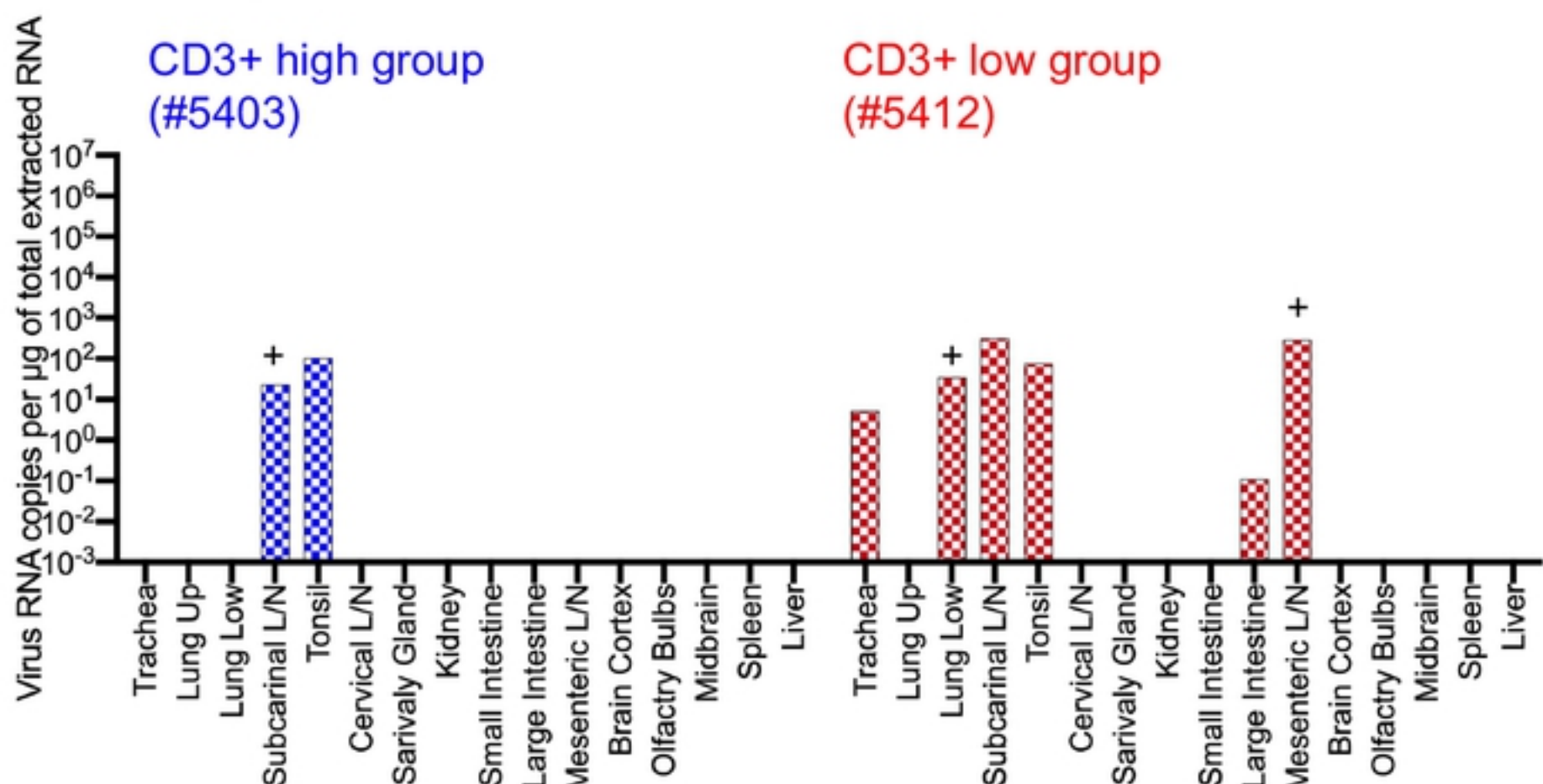
A

7 days p.i.



B

R7 days p.i.



C

R14 days p.i.

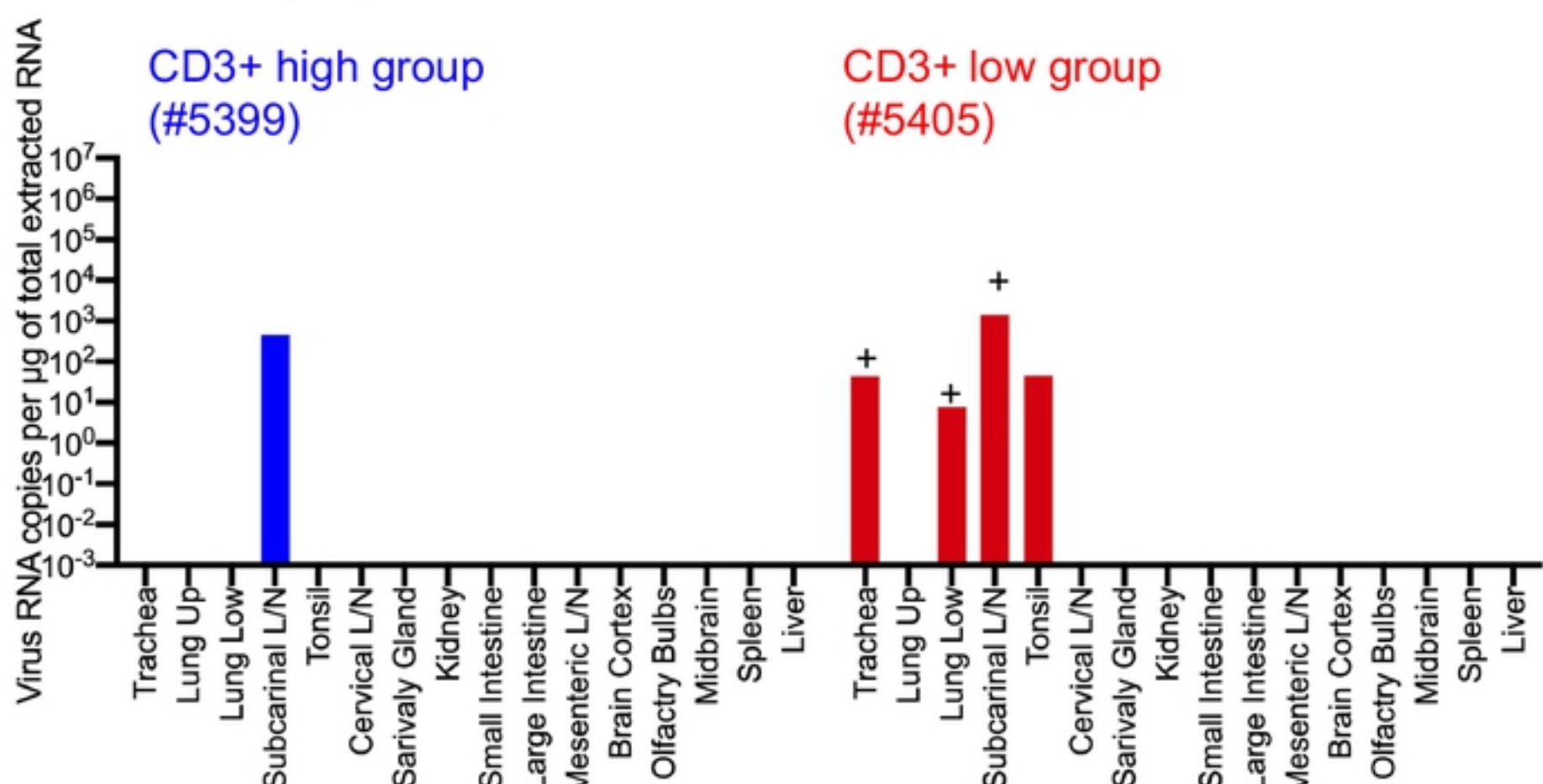
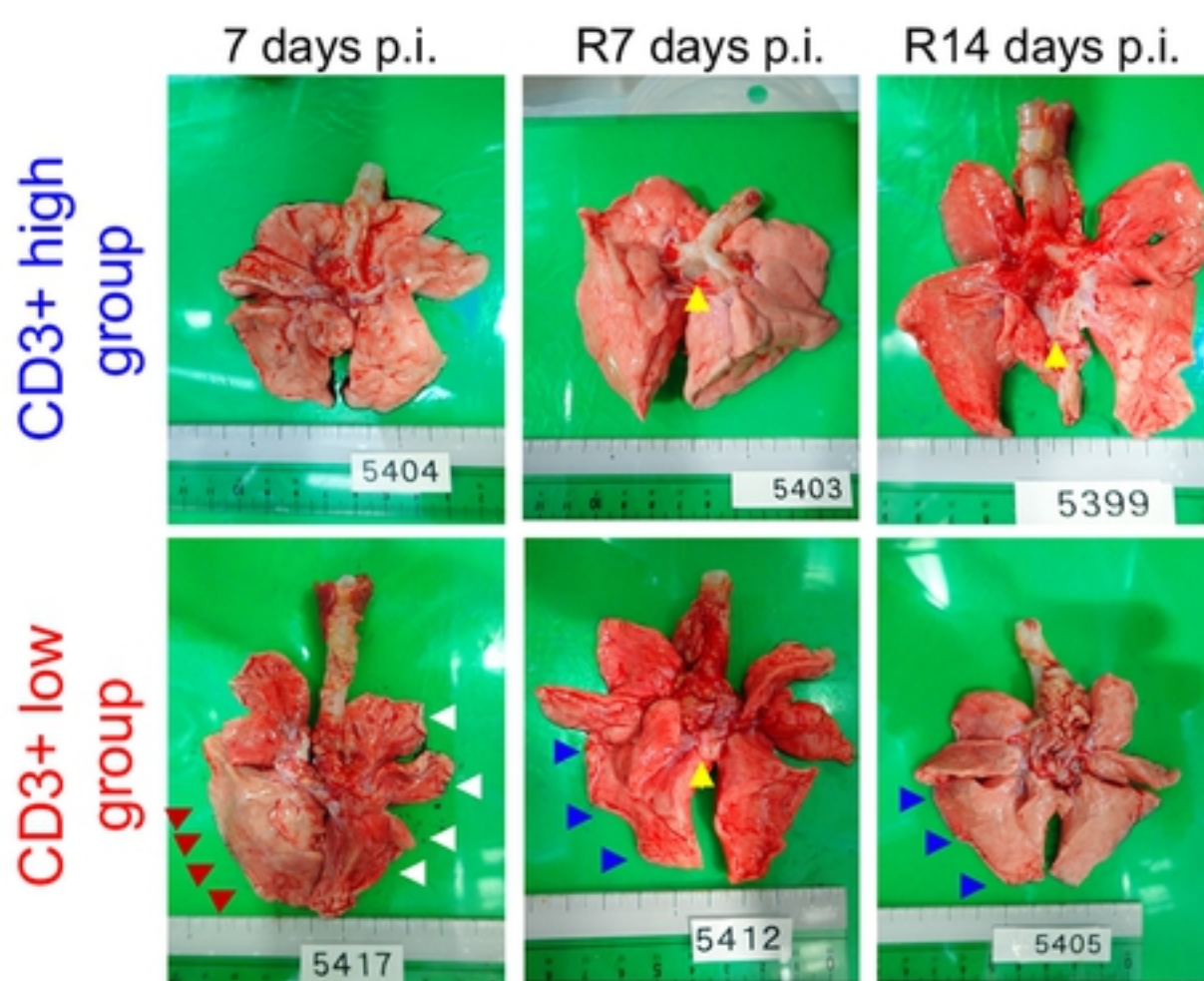
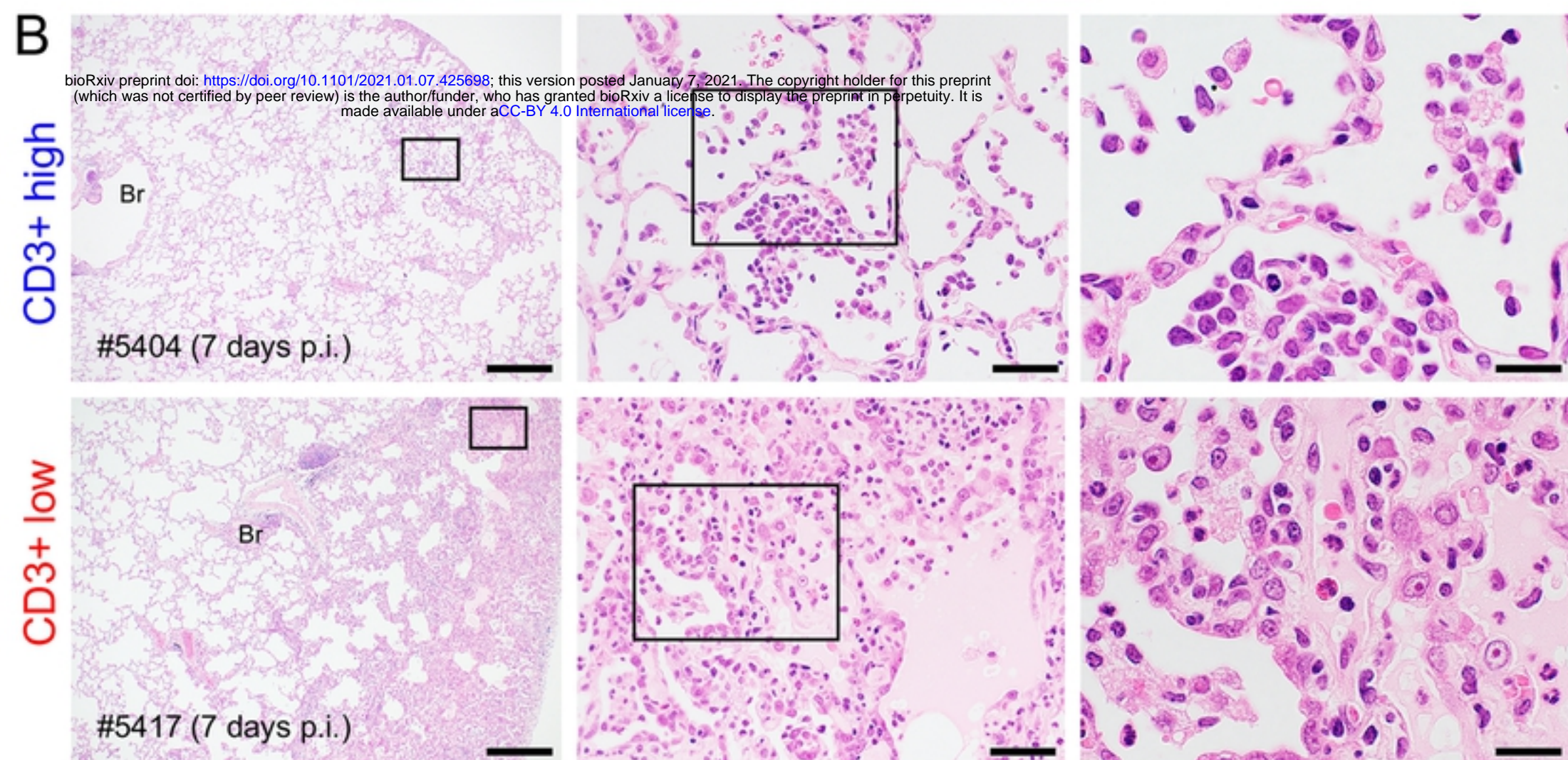
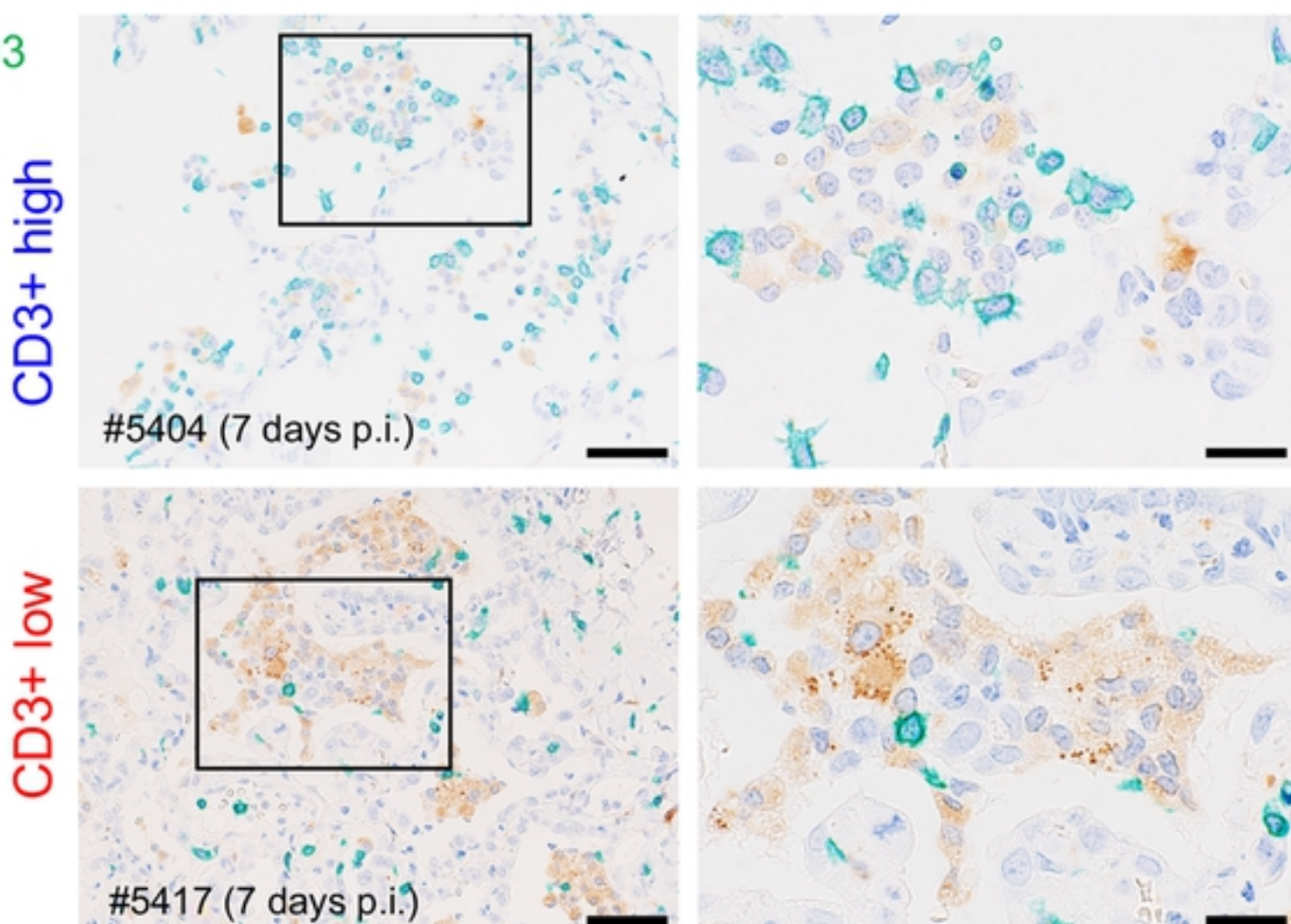


Figure 6

A**B****C****Figure 7**